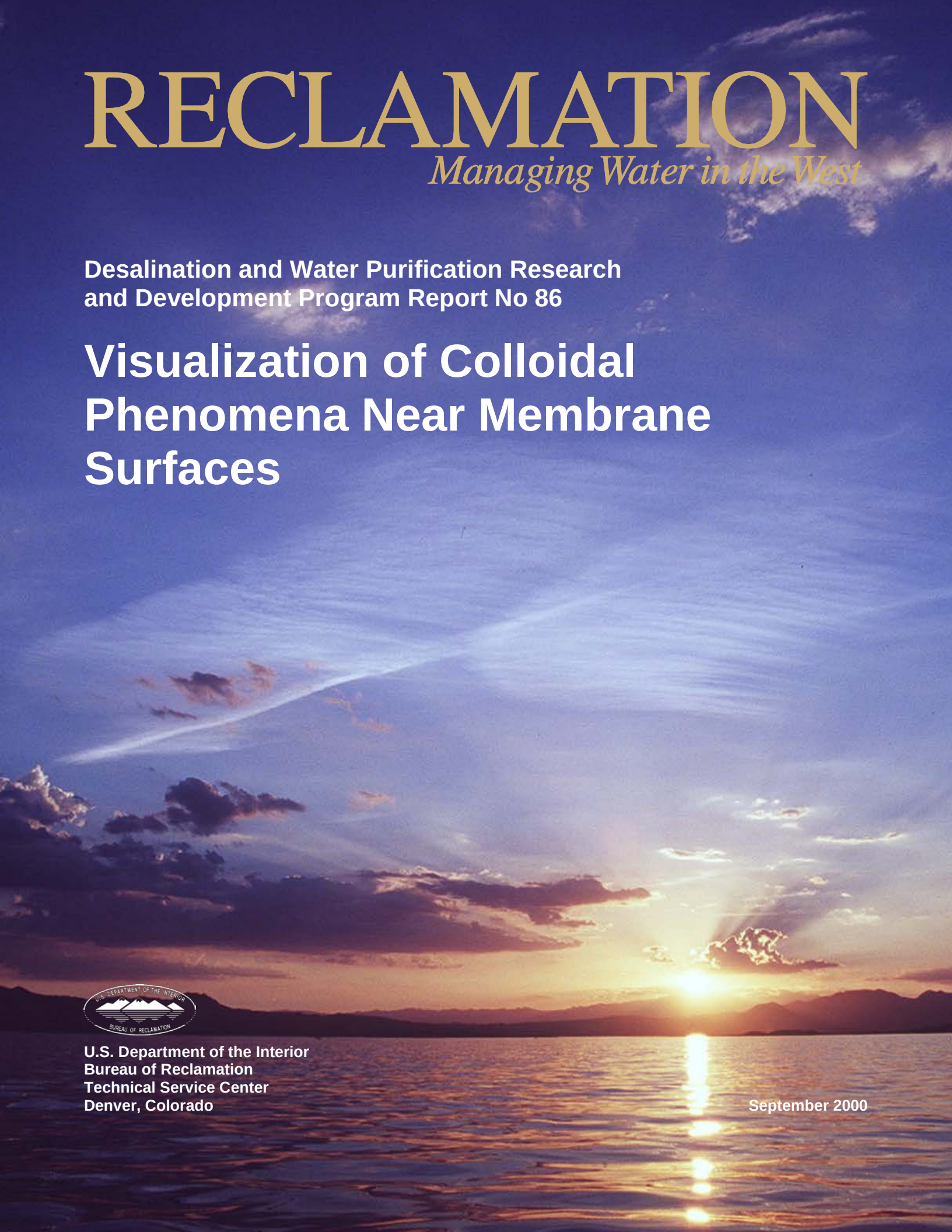

RECLAMATION

Managing Water in the West

Desalination and Water Purification Research and Development Program Report No 86

Visualization of Colloidal Phenomena Near Membrane Surfaces

U.S. Department of the Interior
Bureau of Reclamation
Technical Service Center
Denver, Colorado

September 2000

REPORT DOCUMENTATION PAGE			Form Approved OMB No. 0704-0188
The public reporting burden for this collection of information is estimated to average 1 hour per response, including the time for reviewing instructions, searching existing data sources, gathering and maintaining the data needed, and completing and reviewing the collection of information. Send comments regarding this burden estimate or any other aspect of this collection of information, including suggestions for reducing the burden, to Department of Defense, Washington Headquarters Services, Directorate for Information Operations and Reports (0704-0188), 1215 Jefferson Davis Highway, Suite 1204, Arlington, VA 22202-4302. Respondents should be aware that notwithstanding any other provision of law, no person shall be subject to any penalty for failing to comply with a collection of information if it does not display a currently valid OMB control number.PLEASE DO NOT RETURN YOUR FORM TO THE ABOVE ADDRESS.			
1. REPORT DATE *(DD-MM-YYYY)* September 2000	2. REPORT TYPE Final		3. DATES COVERED *(From - To)* 1999
4. TITLE AND SUBTITLE Visualization of Colloidal Phenomena Near Membrane Surfaces		5a. CONTRACT NUMBER Agreement No. 99-FC-81-0182 5b. GRANT NUMBER 5c. PROGRAM ELEMENT NUMBER	
6. AUTHOR(S) Mark Clark		5d. PROJECT NUMBER 5e. TASK NUMBER 5f. WORK UNIT NUMBER	
7. PERFORMING ORGANIZATION NAME(S) AND ADDRESS(ES) University of Illinois			8. PERFORMING ORGANIZATION REPORT NUMBER
9. SPONSORING/MONITORING AGENCY NAME(S) AND ADDRESS(ES) Bureau of Reclamation U.S. Department of the Interior Denver Federal Center PO Box 25007, Denver, CO 80225-0007			10. SPONSOR/MONITOR'S ACRONYM(S) Reclamation 11. SPONSOR/MONITOR'S REPORT NUMBER(S) DWPR Report No. 86
12. DISTRIBUTION/AVAILABILITY STATEMENT Online at https://www.usbr.gov/research/dwpr/DWPR_Reports.html			
13. SUPPLEMENTARY NOTES			
14. ABSTRACT The objective of this investigation was to systematically investigate the effects of polar (hydrophobic/hydrophilic) interactions on colloidal membrane fouling. To do this, the surface energetics (or more specifically, the polar properties) of several membranes and colloids are measured using the Lifshitz-van der Waals acid-base approach [25, 29]. These results are used in an extended DLVO analysis to evaluate membrane-colloid interactions upon close approach. By comparing the XDLVO results with predictions from the classical DLVO theory for different membrane-colloid combinations, the contribution of polar interactions relative to electrostatic and Lifshitz-van der Waals interactions is examined.			
15. SUBJECT TERMS colloidal fouling. membranes, polar interactions, desalination			

16. SECURITY CLASSIFICATION OF:			17. LIMITATION OF ABSTRACT	18. NUMBER OF PAGES	19a. NAME OF RESPONSIBLE PERSON Yuliana Porras-Mendoza
a. REPORT U	b. ABSTRACT U	THIS PAGE U			19b. TELEPHONE NUMBER *(Include area code)* 303-445-2265

Standard Form 298 (Rev. 8/98)
Prescribed by ANSI Std. Z39.18

Desalination and Water Purification Research and Development Program Report No. 86

Visualization of Colloidal Phenomena Near Membrane Surfaces

Prepared for the Bureau of Reclamation Under Agreement No. 99-FC-81-0182

By

Mark Clark
University of Illinois

U.S. Department of the Interior
Bureau of Reclamation
Technical Service Center
Denver, Colorado

September 2000

Mission Statements

The U.S. Department of the Interior protects America's natural resources and heritage, honors our cultures and tribal communities, and supplies the energy to power our future.

The mission of the Bureau of Reclamation is to manage, develop, and protect water and related resources in an environmentally and economically sound manner in the interest of the American public.

Disclaimer

The views, analysis, recommendations, and conclusions in this report are those of the authors and do not represent official or unofficial policies or opinions of the United States Government, and the United States takes no position with regard to any findings, conclusions, or recommendations made. As such, mention of trade names or commercial products does not constitute their endorsement by the United States Government.

Acknowledgments

The Desalination and Water Purification Research and Development Program, Reclamation, is the sponsor of the research.

Acronyms

°C	Celsuis .
AB	acid-base
CP	concentration polarization
DI	deionized
DLVO	Derjaguin-Landau-Verwey-Overbeek
EDL	electric double layers
EL	electrostatic
IR	infrared
LW	Lifshitz-van der Waals
NF	nanofiltration
NOM	natural organic matter
PS02N	polystyrene microspheres
RO	nonporous reverse osmosis
SEI	surface element integration
UF	ultrafiltration
XDLVO	extended DLVO

Contents

1. Introduction

During the past decade, numerous investigations have focused on elucidation of the mechanisms involved in colloidal membrane fouling (e.g., [1-16]). These investigations generally reveal that colloidal fouling results from the deposition of particles onto membrane surfaces through a combination of physical (hydrodynamic) and chemical (colloidal) interactions [6, 7, 10, 11, 13]. Furthermore, these studies clearly show that while hydrodynamic drag forces bring the particles close to the membrane surface, it is the colloidal (chemical) interactions that cause binding of the particles to the membrane [9, 11].

The chemical interactions leading to colloidal membrane fouling are generally assessed using the classical Derjaguin-Landau-Verwey-Overbeek (DLVO) theory [17], which considers two types of interactions, namely, van der Waals and electrostatic double layer interactions. Quite often, these two interactions alone fail to explain the fouling behavior of a membrane [18]. Under such circumstances, the discrepancy between the theoretical DLVO predictions and experimental observations is typically accounted for using additional mechanisms and hypotheses. For example, these discrepancies have sometimes been attributed to chemical and morphological heterogeneity of the membrane surfaces [10, 19-23], while in other instances, they have been attributed to additional types of interactions between the membranes and foulants [24-27]. It is quite possible that the presence of morphological and chemical heterogeneities can result in surfaces with very different energy distributions than smooth or chemically homogeneous surfaces [10, 24-27], and hence, can result in substantially different fouling behavior compared to theoretical DLVO predictions. Equally likely, however, is the presence of additional interactions between a membrane and a foulant, particularly at very small separations, leading to “aberrant” fouling propensities. For many uncharged materials, the presence of additional interactions induced by the polarity of the solvent has been observed [24-27], and this has led to a school of thought that proposes an extended DLVO (XDLVO) type approach to account for the total interactions in such systems [3, 25, 26, 28-31].

The additional interaction in the XDLVO model is often attributed to a short-ranged acid-base (electron donor/electron acceptor) interaction (possibly stemming from hydrogen bonding) between two surfaces immersed in a polar solvent (e.g., water) [3, 25, 28, 30-33]. This interaction may be attractive (hydrophobic attraction) or repulsive (hydrophilic repulsion). The presence of these interactions is strongly supported by the measurement of surface tensions of various substances. In water, for example, the major contribution (51 mJ/m^2) to the total surface tension (72.8 mJ/m^2) stems from these polar interactions, while the van der Waals contribution (21.8 mJ/m^2) is much lower. Interfacial tension measurements for many polymeric surfaces immersed in water have also revealed a substantial acid-base contribution [4, 18, 29, 34]. The fouling of polymeric membranes is therefore likely to be influenced by acid-base interactions and the contribution of polar interactions to colloidal membrane fouling should be examined.

Comparisons between the DLVO theory and the XDLVO approach have been made in previous investigations concerning deposition and aggregation in aqueous systems (e.g., [29, 31, 35]). Meinders et al. [Meinders, 1995 #55] investigated deposition efficiencies and reversibility of bacterial adhesion on various substratum surfaces and compared those results to DLVO and XDLVO predictions. It was concluded that bacterial adhesion to the surfaces studied was more accurately explained by the XDLVO approach. Ohki and Ohshima [35] analyzed the interaction and aggregation of lipid vesicles using the DLVO and XDLVO models and found that the XDLVO approach was more accurate in describing interactions occurring at a separation distance less than 2 nm, where hydrophobic interactions are strong. Wu et al. [31] examined interactions occurring in particle suspensions and compared experimental results with both DLVO and XDLVO predictions. It was concluded that the XDLVO approach nearly always described the interactions of immersed or dissolved species more accurately than the DLVO theory. The above studies represent a small cross-section of a vast body of evidence showing the considerable influence of polar interactions, particularly at small separations between the interacting surfaces, on particle deposition and attachment. This leads to the question of whether these interactions also influence colloidal membrane fouling and, if so, to what extent.

Several studies use the concept of hydrophilicity and hydrophobicity of membranes to assess their propensity toward fouling. A membrane can be classified as either having a high surface energy (i.e., being hydrophilic) or as having a low surface energy (i.e., being hydrophobic) [14, 25, 36]. In numerous previous investigations (e.g., [34, 37-43]) the hydrophobic nature of a membrane has been estimated from its contact angle with water and correlated with membrane fouling. It has generally been concluded that hydrophobic membranes tend to foul more rapidly than hydrophilic membranes [4, 14, 37, 40-42, 44-49]. This is presumably because hydrophobic membranes prefer to be covered with colloids than with water [4, 50]. Additionally, it has been shown that membrane fouling can be reduced through the hydrophilization of UF [37, 40, 41, 44, 51] and RO [46, 48, 52] membrane surfaces.

Many earlier studies present a somewhat incomplete, and occasionally even misleading picture about the role of polar interactions in membrane fouling. First, only the hydrophobic/hydrophilic nature of the membrane has been considered in many studies when evaluating membrane fouling. However, the hydrophobic/hydrophilic nature of the potential foulant must also be considered when analyzing the influence of polar interactions on colloidal fouling. Second, it is not sufficient to simply relate fouling propensity of a surface to the contact angle of water on that surface. Polar interactions cannot be rigorously quantified solely on the basis of contact angle measurement with water, which merely provides a qualitative estimate of these interactions. To elucidate the influence of polar interactions on colloidal membrane fouling, a systematic characterization of the membrane-colloid system should be performed and a self-consistent analysis that quantifies the polar properties should be used.

The objective of this investigation was to systematically investigate the effects of polar (hydrophobic/hydrophilic) interactions on colloidal membrane fouling. To do this, the surface energetics (or more specifically, the polar properties) of several membranes and

colloids are measured using the Lifshitz-van der Waals acid-base approach [25, 29]. These results are used in an extended DLVO analysis to evaluate membrane-colloid interactions upon close approach. By comparing the XDLVO results with predictions from the classical DLVO theory for different membrane-colloid combinations, the contribution of polar interactions relative to electrostatic and Lifshitz-van der Waals interactions is examined.

2. Background and Related Research

2.1. Membrane-Colloid Interaction

Colloids are transported to a membrane surface, in cross-flow operation of NF and RO membranes, by several transport mechanisms: diffusion, transverse transport due to permeation drag and inertial lift, and transport due to gravitational, van-der Waals, and double layer forces [15, 53, 54]. The transport of colloids to the membrane surface, results in the formation of a cake layer over time for RO membranes [15]. The colloids accumulate on a membrane surface or in its pores [6, 54]. Although pore plugging is a predominant fouling parameter in porous membranes it is not a consideration for RO membranes as they are non-porous [6]. Therefore, the sole mechanism of RO colloidal fouling is cake layer formation [53].

Cake layer formation occurs as suspended particles are transported to the membrane surface by the permeate flow, thus forming a concentration polarization (CP) layer [11]. Particle concentration increases with time before reaching a maximum value, forming a cake layer between the membrane and CP layer. As particles continue to be transported to the membrane surface the cake layer growth occurs until a steady-state is reached. Steady-state indicates that the transport of particles from the bulk solution to the CP layer by the transverse permeate flow is balanced by the longitudinal transport of particles by the cross flow. On a macro-scale, the rate of cake layer formation is controlled by various operating parameters such as permeate flux rate, cross-flow velocity, applied pressure, feed colloid concentration, and average particle size [15]. Various models have been developed for cake layer growth, taking into account those macro-parameters just mentioned [15, 54]. On a micro-scale, it has been theorized that membrane-colloid interaction, as well as the interaction between suspended and retained colloids may also play a substantial role in controlling cake layer formation [3, 6, 55]. In this respect, the interaction between a colloid and membrane has been described using the Derjaguin-Landau-Verwey-Overbeek (DLVO) theory [20]. The magnitude and sign of the interaction parameter is a measure of the total interaction energy between the membrane and colloid immersed in an aqueous environment, and can be used to quantify the favorability of adhesion between the two surfaces [3]. The DLVO theory expresses the total interaction energy, or energy of adhesion, between a colloid and a membrane as the sum of the attractive Lifshitz-van der Waals (LW) and electrostatic (EL) interaction energies according to Equation 1:

$$U_{mlc}^{DLVO} = U_{mlc}^{LW} + U_{mlc}^{EL} \quad \textbf{(1)}$$

where U^{DLVO} is the total interaction energy between the membrane and colloid immersed in water, U^{LW} is the Lifshitz-van der Waals interaction term, and U^{EL} is the electrostatic interaction term. The subscripts *m, l,* and *c* correspond to the membrane, bulk feed solution, and colloid, respectively.

It has been suggested by van Oss [1993] [25] that any energy balance performed for an aqueous system must, in addition to including the Lifshitz-van der Waals (LW) and electrostatic (EL) interaction energies, also include the acid-base (AB) interaction energy. Inclusion of the AB interaction term into the DLVO approach results in the XDLVO approach, which may written as Equation 2:

$$U_{mlc}^{XDLVO} = U_{mlc}^{LW} + U_{mlc}^{EL} + U_{mlc}^{AB} \quad \textbf{(2)}$$

where U^{XDLVO} is the total interaction energy between the membrane and colloid immersed in water and U^{AB} is the acid-base interaction term.

Application of the XDLVO theory requires that the surface energy parameters of the membrane and colloid be experimentally determined, with such values for various liquids previously known. Surface energy data can be calculated for membranes and colloids using contact angle data and the Lifshitz-van der Waals acid-base approach [25, 29]. The acid-base approach relates contact angle data and the known surface energy properties of the contact angle liquid(s) to the surface energy parameters of the membrane. By determining surface energy properties for both membrane surfaces and model colloidal foulants the XDLVO theory may be used to better understand the transport of a colloid to a membrane surface, and hence, a better understanding of fouling mechanisms is gained.

2.2. Solid Surface Characterization

2.2.1. Contact Angle

Solid surface characterization is based on the relatively simple, yet complex, contact angle concept. Contact angle is a measure of the wettability of a solid surface [36, 43, 56-60]. Surface wettability is defined as the ability of the surface to adsorb water [43]. Wettability can be interpreted as the hydrophobicity or hydrophilicity of a surface [43]. In other words, a contact angle of 0˚ would correspond to an ideal hydrophilic surface, while a contact angle of 180˚ would correspond to an ideal hydrophobic surface. Contact angle can also be used to determine the surface tension components of a solid surface [36]. When a drop of liquid is placed on a dry membrane surface, the contact angle is the angle that develops between the membrane surface and the vapor/liquid interface. The contact angle is formed at the junction of the three phases (i.e., the solid, liquid and gas phases)

and is measured through the denser fluid phase [43]. Figure 1 illustrates the contact angle of a liquid drop on a solid surface; the contact angle is measured through the liquid phase.

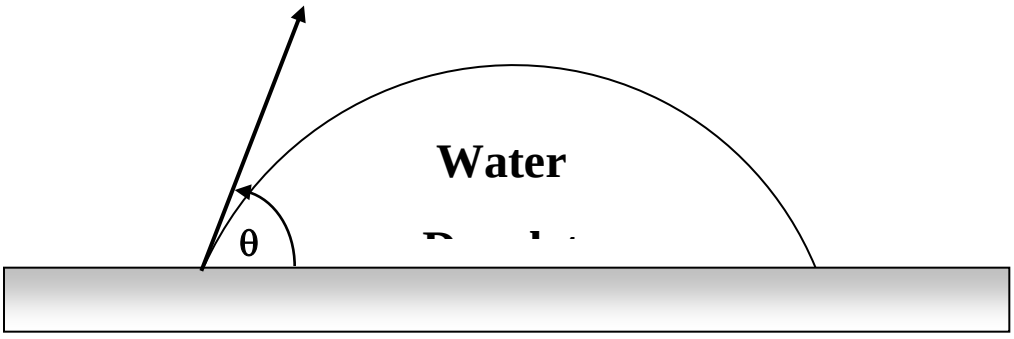

Figure 1. Contact angle of a liquid drop on a solid surface (the sessile drop technique).

The theory of interfacial tensions began with Young's equation (Equation 3), which is obeyed at the triple interface between solid, liquid and vapor phases [25].

$$\gamma_s^{TOT} - \gamma_{sl}^{TOT} - \pi_e = \gamma_l^{TOT} \cos\theta \quad \textbf{(3)}$$

where γ_s^{TOT} is the total free energy of the solid phase; γ_l^{TOT} is the total free energy of the liquid phase; γ_{sl}^{TOT} is the interfacial tension between the solid and the liquid; π_e is the equilibrium interfacial film pressure; and θ is the equilibrium contact angle.

Equilibrium spreading pressure results from the condensation of the probe liquid and its subsequent deposition on the solid surface [25]. Spreading pressure may be neglected for high-energy liquids (i.e., $\gamma_l > \gamma_s$) [25]. As membrane probe liquid combinations used in this investigation meet this requirement (i.e., $\gamma_l > \gamma_s$), spreading pressure is neglected in these surface energy calculations. Therefore, when neglecting spreading pressure, Young's equation is written as Equation 4:

$$\gamma_s^{TOT} - \gamma_{sl}^{TOT} = \gamma_l^{TOT} \cos\theta \quad \textbf{(4)}$$

Young's equation illustrates the relationship between the adhesion of the liquid to the solid surface and the cohesion of the liquid to itself [61, 62]. In Young's equation, the term $\gamma_l \cos\theta$ is often referred to as the wetting tension, or the adhesion tension [36]. In other words, this term gives the surface tension value for the liquid solution at which it will wet, or adhere to, the solid surface. When the self-cohesion of the liquid is greater than the adhesion of the liquid to the solid, a large contact angle is formed [62]. As the

self-cohesion of the liquid decreases the contact angle that the liquid forms on the solid decreases [62]. When the adhesion of the liquid to the solid is much greater than the self-cohesion of the liquid, a small contact angle is formed.

2.2.2. Fowkes' Approach

Until recently, the solid surface tension has been considered experimentally inaccessible because the first term in Young's equation cannot be separated into its γ_s and γ_{sl} components. Therefore, only the difference between the two solid surface tension parameters is experimentally accessible. Recently attempts have been made to formulate a mathematical relationship in order to calculate the individual solid surface tension values [25, 63, 64]. Such relationships utilize the known surface energy values of a liquid and an energy balance between the solid and liquid in order to calculate the solid surface tension values [25]. The first to use such a method was Fowkes [1964][65]. Fowkes [1964] stated that the total surface energy of a respective phase (solid or liquid) can be expressed as a summation of its two surface energy components Equation 5:

$$\gamma^{TOT} = \gamma^{d} + \gamma^{n} \tag{5}$$

where γ^{TOT} is the total surface free energy; γ^{d} is the dispersive surface energy component and γ^{n} is the non-dispersive surface energy component. The dispersive energy component specifically results from molecular interaction due to London forces. The non-dispersive energy component is an inclusive term describing all interactions due to non-London intermolecular forces [25]. Non-London forces include hydrogen and dipole-dipole interactions.

Using Equation 5, the interaction between two phases, a solid and a liquid, can be expressed using a geometric mean relationship for the dispersive energy components of the solid and liquid phases as shown in Equation 6:

$$\gamma_{sl}^{TOT} = \gamma_{s}^{TOT} + \gamma_{l}^{TOT} - 2\sqrt{\gamma_{s}^{d}\gamma_{l}^{d}} \tag{6}$$

where γ_s^{d} is the dispersive surface energy component of the solid and γ_l^{d} is the dispersive surface energy component of the liquid. Inserting Equation 6 into Young's equation (Equation 4) produces Equation 7:

$$\gamma_{l}^{TOT}\cos\theta = -\gamma_{l}^{TOT} + 2\sqrt{\gamma_{s}^{d}\gamma_{l}^{d}} \tag{7}$$

Applying Equation 7 to actual systems provides a means to calculate the surface energy properties of a solid surface using the known surface properties of a liquid and the contact angle of the liquid with the solid. However, as evident from Equation 7, Fowkes' [1964] method only applies to solid surfaces that are strictly dispersive ($\gamma_s = \gamma_s^d$). Therefore, this method is rather limited in its ability to characterize typical solid surfaces.

2.2.3. Lifshitz-van der Waals/Acid-Base Approach

A generalization of the Fowkes approach to surface characterization was developed by van Oss et al. [1986] and used to calculate the energy (or force) per unit area between two parallel infinitely long plates. van Oss et al. [1986] simplified the general surface energy components proposed by Fowkes [1964]. The dispersive forces cited by Fowkes are ascribed solely to the apolar Lifshitz-van der Waals (LW) surface energy component, which are considered to control physical molecular interactions. In an aqueous environment LW forces are always attractive [3, 18, 25, 66]. Attractive forces are represented by negative values, while a positive value designates a repulsive force. The non-dispersive forces cited by Fowkes are ascribed to polar acid-base (AB) interactions at a surface due to hydrogen bonding. Acid-base interactions, which act over a shorter range than LW forces, result from electron/proton exchange [3]. Acid-base forces control the chemical interactions relevant to wetting behavior, and have also been described as hydration pressure, hydrogen bonding, and hydrophobic attraction. Unlike LW forces, AB forces may be either repulsive (positive value) or attractive (negative value). Typically, however, AB forces are repulsive for extremely hydrophilic surfaces immersed in water. The result is Equation 8, the expression for the total free energy of adhesion for a surface:

$$\gamma^{TOT} = \gamma^{LW} + \gamma^{AB} \quad \textbf{(8)}$$

where γ^{LW} is the Lifshitz-van der Waals component of surface energy and γ^{AB} is the acid-base component of surface energy. This modification is referred to as the Lifshitz-van der Waals/Acid-Base approach. The Lifshitz-van der Waals/Acid-Base approach has been widely used as a method for determining surface tension components of a solid and interfacial free energies between two phases [64].

The non-polar LW force represents a single electrodynamic property of a given material. Conversely, the polar AB force is comprised of two non-additive electron-acceptor and electron-donor components [25]. The polar AB component of a material's surface energy is thus given by [34, 67] and expressed in Equation 9:

$$\gamma^{AB} = 2\sqrt{\gamma^{+}\gamma^{-}} \quad \textbf{(9)}$$

where γ^{+} is the electron-acceptor component and γ^{-} is the electron-donor component. The electron-acceptor component represents the acidic character and the electron-donor

component the basic character of a respective surface [25]. Investigations employing the van der Waals acid-base approach to surface characterization, have found most surfaces to be basic with a small or negligible acid component. Substituting Equation 9 into Equation 8 produces Equation 10 for the total surface energy of a respective phase:

$$\gamma^{TOT} = \gamma^{LW} + 2\sqrt{\gamma^{+}\gamma^{-}} \quad \textbf{(10)}$$

Division of the AB force into two components demonstrates the fact that a polar liquid molecule may be adsorbed onto a polar surface either by its positive or negative pole [34]. The polar interaction between two particles (particle 1 and particle 2) is described based on these two components. The electron-acceptor of particle 1 interacts with the electron-donor of particle 2 and the electron-donor of particle 1 interacts with the electron-acceptor of particle 2 [25]. Therefore, the polar interfacial free energy existing between particles 1 and 2 can be expressed by Equation 11 [68]:

$$\Delta G_{12}^{AB} = -2\left(\sqrt{\gamma_1^{+}\gamma_2^{-}} + \sqrt{\gamma_1^{-}\gamma_2^{+}}\right) \quad \textbf{(11)}$$

where ΔG_{12}^{AB} is the free energy of interaction between polar materials 1 and 2; γ_1^{+} is the electron-acceptor component of particle 1; γ_2^{+} is the electron-acceptor component of particle 2; γ_1^{-} is the electron-donor component of particle 1; and γ_2^{-} is the electron-donor component of particle 2. Using the Dupre equation, the interaction between two polar surfaces can be expressed as Equation 12:

$$\gamma_{12}^{AB} = \Delta G_{12}^{AB} + \gamma_1^{AB} + \gamma_2^{AB} \quad \textbf{(12)}$$

where γ_{12}^{AB} is the acid-base interaction energy between particles 1 and 2; γ_1^{AB} is the acid-base energy component of particle 1; and γ_2^{AB} is the acid-base energy component of particle 2. Substituting Eqs. 9 and 11 into Eq. 12 yields the Equation 13 for the polar interfacial free energy between particles 1 and 2:

$$\gamma_{12}^{AB} = 2\left(\sqrt{\gamma_1^{+}\gamma_1^{-}} + \sqrt{\gamma_2^{+}\gamma_2^{-}} - \sqrt{\gamma_1^{+}\gamma_2^{-}} - \sqrt{\gamma_1^{-}\gamma_2^{+}}\right) \quad \textbf{(13)}$$

The apolar (LW) interfacial free energy between particles 1 and 2 may be expressed using Equation 14 [25]:

$$\gamma_{12}^{LW} = \left(\sqrt{\gamma_1^{LW}} - \sqrt{\gamma_2^{LW}}\right)^2 \quad \textbf{(14)}$$

where γ_{12}^{LW} is the Lifshitz-van der/Waals Acid-Base interfacial free energy between particles 1 and 2; γ_1^{LW} is the apolar energy component of particle 1; and γ_2^{LW} is the apolar energy component of particle 2. Substituting Equations. 13 and 14 into Equation 8 produces Equation 15 for the total interfacial free energy between particles 1 and 2:

$$\gamma_{12} = \left(\sqrt{\gamma_1^{LW}} - \sqrt{\gamma_2^{LW}}\right)^2 + 2\left(\sqrt{\gamma_1^+\gamma_1^-} + \sqrt{\gamma_2^+\gamma_2^-} - \sqrt{\gamma_1^+\gamma_2^-} - \sqrt{\gamma_1^-\gamma_2^+}\right) \quad \textbf{(15)}$$

where γ_{12} is the total interfacial tension between particles 1 and 2. Combining Equations. 8, 9, 10, and 14 results in Equation 16 for the interfacial free energy between a solid and a liquid:

$$\Delta G_{sl} = 2\left(\sqrt{\gamma_s^{LW}\gamma_l^{LW}} + \sqrt{\gamma_s^+\gamma_l^-} + \sqrt{\gamma_s^-\gamma_l^+}\right) \quad \textbf{(16)}$$

where ΔG_{sl} is the interfacial free energy between a solid and a liquid; γ_s^{LW} is the Lifshitz-van der Waals component of the solid phase; γ_l^{LW} is the Lifshitz-van der Waals component of the liquid phase; γ_s^+ is the electron-acceptor component of the solid phase; γ_s^- is the electron-donor component of the solid phase; γ_l^+ is the electron-acceptor component of the liquid phase; and γ_l^- is the electron-donor component of the liquid phase. The interaction between a solid and a liquid can also be described in terms of the contact angle between them. Equation 17 is known as the Young-Dupre equation [25]:

$$-\Delta G_{sl} = (1 + \cos\theta)\gamma_l^{TOT} \quad \textbf{(17)}$$

where γ_l^{TOT} is the total free energy of the liquid and ΔG_{sl} is the Gibbs energy of adhesion between a solid and a liquid. Combining Equations. 14 and 15 results in the Extended Young equation (Equation 18), which relates the contact angle of a liquid on a solid surface to the surface energy parameters of both the solid and the liquid [4, 34, 68]:

$$(1 + \cos\theta)\gamma_l^{TOT} = 2\left(\sqrt{\gamma_s^{LW}\gamma_l^{LW}} + \sqrt{\gamma_s^+\gamma_l^-} + \sqrt{\gamma_s^-\gamma_l^+}\right) \quad \textbf{(18)}$$

The Extended Young (Equation 18) is best described as an equilibrium force balance. The left hand side, or the free energy of cohesion of the liquid (l), is equal to the right hand side, or the free energy of adhesion between the liquid (l) and the solid (s) [25, 61]**.** Based on the Extended Young equation, the surface energy parameters of a solid surface (γ_s^{LW}, γ_s^+, γ_s^-) can be determined by performing contact angle measurements using three probe liquids with known surface energy parameters (γ_l^{LW}, γ_l^+, γ_l^-), [25]. Two of the probe liquids should be polar and one of the probe liquids should be apolar. The apolar liquid is used to calculate the non-polar, γ_s^{LW} component of a solid [25]. Furthermore, high energy (apolar and polar) liquids are recommended to improve contact angle accuracy due to the large contact angles that are formed.

2.2.4. Deviations from Young's Equation

Young's equation was developed for an ideal solid surface [36, 39]. An ideal solid surface must be smooth at the molecular level, chemically homogeneous, rigid, non-reactive, and insoluble [36, 39, 69]. The contact angle of a pure probe liquid on an ideal

surface is called the intrinsic contact angle, or the true contact angle, for the given solid [69]. It is only when an ideal solid surface and a pure liquid are used, that Young's equation is truly descriptive of the solid's surface energetics.

With the exception of cleaved mica, ideal surfaces are very rare [36]. Most surfaces have some degree of heterogeneity and roughness. Chemical heterogeneity of a solid surface creates strips of wettable (hydrophilic) and non-wettable (hydrophobic) areas [70]. A liquid droplet will align itself on those areas that are the most hydrophilic or wettable, thus creating the condition where the observed contact angle is not representative of the true surface [71]. This facilitates a condition where the surface energy is not the sole determiner of the observed contact angle.

The presence of pores and the physical roughness of a membrane surface also cause the measured contact angle to deviate from the intrinsic contact angle [72-74]. The apparent contact angle is most often measured. The apparent contact angle does not account for surface roughness [64]. Membrane surface roughness may be on the order of several micrometers [Keurentjes et al. 1989] [71] and can be increased through improper handling. As the liquid advances on an inclined surface (e.g., the ridge of a rough surface), a larger apparent contact angle is formed [71]. The apparent contact angle becomes larger as the edge of the liquid drop becomes more horizontal as it travels up the incline of the surface indentation or elevation. Furthermore, as membrane surface roughness increases it becomes more difficult to describe membrane-colloid interaction by a single interaction energy value, instead a distribution of interaction energies must be considered [53].

Deviations from an ideal surface may also result from contamination during the construction and handling of the membrane. Surface contaminants often bear little resemblance to the bulk solid and can therefore lead to increased chemical heterogeneity [53]. Surface contamination may also lead to increased surface roughness.

2.2.5. Interaction Energy Between a Spherical Colloid and an Infinite Planar Surface

For evaluating colloidal systems, where colloids are considered spherical or equivalent spheres, the interaction energy between a flat surface and spherical particles must be determined [55]. In order to calculate the interaction energy between a membrane, considered an infinitely long planar surface, and a colloid, which is considered a perfect sphere, Derjaguin's approximation must be used, as shown in Equation 19:

$$\Delta G_{i(y)} = f(a)\int_{y}^{\infty} \Delta G_i(l)\,dl \qquad \textbf{(19)}$$

where a is the radius of the colloid; $f(a)$ is a geometrical factor representing the curvature of the colloid; $\Delta G_i(l)$ represents the interaction energy per unit area between two planar surfaces separated by distance l; and d is the distance of closest approach between the

colloid and the membrane surface. The term *i* corresponds to LW, EL, or AB, depending on which term is evaluated.

Surface tension values for the membranes and colloids calculated using the Lifshitz-van der Waals acid/base approach can be used in Derjaguin's approximation to calculate van der Waals (LW) and acid-base (AB) interfacial free energies at the equilibrium cut-off distance between a membrane and a colloid (ΔG_{y0}) [29]. Expressions for the LW and AB interaction energies at the point of contact are shown in Equations 20 and 21:

$$\Delta G_{y_0}^{LW} = -2\left(\sqrt{\gamma_l^{LW}} - \sqrt{\gamma_m^{LW}}\right)\left(\sqrt{\gamma_l^{LW}} - \sqrt{\gamma_c^{LW}}\right) \tag{20}$$

$$\begin{aligned}\Delta G_{y_0}^{AB} = {} & 2\sqrt{\gamma_l^+}\left(\sqrt{\gamma_m^-} + \sqrt{\gamma_c^-} - \sqrt{\gamma_l^-}\right) + 2\sqrt{\gamma_l^-}\left(\sqrt{\gamma_m^+} + \sqrt{\gamma_c^+} - \sqrt{\gamma_l^+}\right) \\ & - 2\sqrt{\gamma_m^+\gamma_c^-} - 2\sqrt{\gamma_m^-\gamma_c^+}\end{aligned} \tag{21}$$

where y_0 represents the distance between the two interacting surfaces. At the point of contact y_0 is equal to 0.158 nm (± 0.009 nm) and may be regarded as the distance between the outer electron shell boundaries (van der Waals boundaries) of adjoining non-covalently interacting molecules [18, 75]. At this minimum distance the divergence of the LW interaction energy between two particles of the same material at contact is prevented [25].

As the separation distance between two surfaces increases, the LW and AB interaction energy components diminish from their corresponding adhesion energy (i.e., the interaction energy at contact given by Equations. 20 and 21) following a unique decay pattern. The LW interaction energy per unit area decays with the inverse square of the distance between two infinite planar surface [68] as shown in Equation 22:

$$\Delta G_{(plate-plate)}^{LW} = -\frac{A}{12\pi y^2} \tag{22}$$

where *A* is the Hamaker constant and *y* is the separation distance between the two interacting planar surfaces. The Hamaker constant can be calculated from the LW component of the free energy of adhesion by rearranging Equation 22 as shown in Equation 23:

$$A = -12\pi y_0^2 \Delta G_{y_0}^{LW} \tag{23}$$

Estimates of free energy of adhesion obtained from the surface tension components provide information about interaction energy per unit area between two infinite planar surfaces. To obtain the actual interaction energy between the membrane (assumed to be an infinite planar surface) and the colloidal particle (assumed to be a sphere), a technique

that converts the interaction energy per unit area to the total interaction energy for a given geometry is required. Derjaguin's technique was therefore used to scale the interaction energy per unit area between two infinite flat surfaces to the corresponding interaction energy between a flat sheet (membrane) and a sphere (colloid). Applying this technique to Equation 8, the LW interaction energy between an infinite flat plate and a spherical colloid is shown in Equation 24:

$$U^{LW}_{(plate-sphere)} = -\frac{Aa_c}{6h} \tag{24}$$

where a_c is the radius of the spherical colloid and h is the surface to surface separation distance between the flat plate (membrane) and the sphere (colloid). Combining Equations. 23 and 24 gives Equation 25, the expression for the LW interaction energy between a membrane and a colloid in an aqueous environment:

$$U^{LW}_{mlc}(h) = 2\pi \Delta G^{LW}_{y_0} \frac{y_0^2 a_c}{h} \tag{25}$$

The expression for the acid-base interaction energy as a function of separation distance is derived similarly. The acid-base interaction energy per unit area decays exponentially with separation distance between two infinite planar surfaces (Equation 26 [3]):

$$\Delta G^{AB}_{(plate-plate)} = \Delta G^{AB}_{y_0} exp\left[\frac{y_0 - y}{\lambda}\right] \tag{26}$$

where λ is the characteristic decay length of AB interactions in water, whose value is between 0.2 and 1.0 nm [76]. A commonly used value of λ for aqueous systems is 0.6 nm [18, 77]; this value was used in the current investigation. Applying Derjaguin's technique to the above equation, the decay behavior of AB interactions between a membrane and a colloid in an aqueous environment is shown in Equation 27:

$$U^{AB}_{mlc}(h) = 2\pi a_c \lambda \Delta G^{AB}_{y_0} exp\left[\frac{y_0 - h}{\lambda}\right] \tag{27}$$

The electrostatic interaction energy per unit area between two infinite planar surfaces decays with separation distance according to Equation 28 [78]:

$$\Delta G^{EL}_{(plate-plate)} = \frac{\varepsilon_0 \varepsilon_r \kappa}{2}\left(\zeta_m^2 + \zeta_c^2\right)\left(1 - coth(\kappa y) + \frac{2\zeta_m \zeta_c}{\left(\zeta_m^2 + \zeta_c^2\right)} csch(\kappa y)\right) \tag{28}$$

where $\varepsilon_0\varepsilon_r$ is the dielectric permittivity of the suspending fluid; κ is the inverse Debye screening length; and ζ_m and ζ_c are the surface potentials of the membrane and colloid, respectively. Once again, applying Derjaguin's technique to Equation 28, the decay

behavior of the EL interaction energy between a membrane and a colloid in an aqueous environment is provided in Equation 29:

$$U_{mlc}^{EL}(h) = \pi\varepsilon_r\varepsilon_0 a_c \left(2\zeta_c\zeta_m \ln\left(\frac{1+e^{-\kappa h}}{1-e^{-\kappa h}}\right) + \left(\zeta_c^2 + \zeta_m^2\right)\ln\left(1-e^{-2\kappa h}\right)\right) \quad \textbf{(29)}$$

In the current investigation, the surface potentials were assumed to be the same as the measured zeta potentials of the surfaces involved. The zeta potentials of the membranes were determined from streaming potential measurements while the zeta potentials of the colloids were determined from electrophoretic mobility measurements. For both membranes and colloids, zeta potential values at pH 5.6 were used to determine the EL interaction energy term. The inverse Debye screening length was determined using the relationship in Equation 30 [5]:

$$\kappa = \sqrt{\frac{e^2 \sum n_i z_i^2}{\varepsilon_r\varepsilon_0 kT}} \quad \textbf{(30)}$$

where e is the electron charge; n_i is the number concentration of ion i in the bulk solution; z_i is the valence of ion i; k is Boltzmann's constant; and T is absolute temperature. For this investigation a background electrolyte of 0.01 M NaCl was assumed.

When a solid is immersed in an aqueous environment a tendency exists for it to acquire an electrical surface charge. At a neutral pH (~ 7.0) most solid surfaces possess a net negative charge. A redistribution of ions in solution occurs as a surface acquires charge. The ions of opposite charge (counter-ions) are attracted to the charged surface, while ions of the same sign (co-ions) are repelled. An electrical double layer is thus created at the proximity of the charged surface. Charged surfaces of like sign are thus repelled by each other. Electrostatic double layer (EL) interactions make a substantial contribution to the total free energy of interaction when solute molecules possess large electrical potentials and relatively weak polar interactions [3]. Energy barriers inhibiting particle attachment or coagulation are attributed to interacting electric double layers (EDL) of like charged surfaces in addition to hydration forces or steric effects [3]. EDL repulsion is a long-range force, significant for a separation distance of approximately 10 nm.

2.2.6. Potential Energy Curve

Equations 25, 27, and 29 may be used to derive an energy distance or potential energy curve for the LW, AB, and EL interaction energies. Potential energy curves graphically illustrate how the three interaction energies act over a given distance from the membrane surface. Summing the three interaction energies produces an XDLVO curve representing how the total interaction energy between a colloid and membrane, based on the XDLVO theory, acts over a specific distance. Potential energy curves are characterized by the presence of a shallow, secondary minimum at longer distances of separation (several hundred Å), an interaction barrier closer to the surface, and a deep, primary interaction

minimum at short distances of separation (< 10 Å) [29]. It has been theorized that particles become reversibly captured in the secondary interaction minimum before becoming irreversibly captured as the bond strengthens with time in the primary interaction minimum [29].

2.2.7. Zeta Potential

The interaction of colloidal particles with a membrane surface is highly dependent on the surface charge of the membrane and colloid [79]. Because surface charge cannot be measured directly for either membranes or colloids, it is commonly quantified in terms of zeta potential. Zeta potential is the electric potential at the shear plane of the electrochemical double layer (between the compact layer and the mobile diffuse layer) [80]. When a membrane is placed in an aqueous environment it acquires a surface charge, either positive or negative, while most colloids are negatively charged [79]. Distribution of ions at the membrane-solute interface is controlled by membrane surface charge, for instance, co-ions are repelled while counter-ions are attracted to the membrane surface. Therefore, an electrochemical double layer (EDL) is formed at a membrane's surface when the membrane is immersed in an ionic solution. The strength of the EDL controls how strongly a colloid is attracted or repelled by the membrane surface. Because most surfaces in aqueous environments are negatively charged, EDL interactions are typically repulsive. Zeta potential for membranes and colloids are measured using different techniques. Streaming potential measurements are used to calculate membrane zeta potential, while electrophoretic mobility measurements are used to calculate zeta potential for colloids.

Electrokinetic properties (zeta potential) of a membrane surface are quantified using streaming potential measurements [79, 80]. Streaming potential is the potential induced when an electrolyte solution flows across a stationary, charged surface (i.e., a membrane surface) under a pressure gradient [79, 80]. Charges in the mobile diffuse layer are carried to one end of the membrane, creating a convective current. As charges accumulate at the end of the membrane an electrical field is established causing a conduction current in the opposite direction. When the convective current equals the conduction current, a steady state is reached. The streaming potential is measured as the electrical potential difference on opposite ends of the membrane per unit of applied pressure [80].

Streaming potential is related to zeta potential through several mathematical relationships. Application of each equation is dependent upon membrane pore structure [80]. For an ideal case (i.e., circular pores) zeta potential is linked to streaming potential using the relationship shown in Equation 31:

$$SP = \frac{\varepsilon_0 \varepsilon_r \zeta}{\eta\left(\lambda_0 + \frac{2\lambda_s}{r}\right)} \quad \textbf{(31)}$$

where ε_0 is the vacuum permittivity; ε_r is the relative dielectric constant of the solvent; η is the viscosity of the solution; λ_0 is the conductivity of the electrolyte in the bulk; λ_s is the surface conductivity; and r_{pore} is the pore radius. Based on Equation 30, the Helmholtz-Smoluchowski relationship can be derived by neglecting the surface conductivity (λ_s) as shown in Equation 32:

$$SP = \frac{\varepsilon_0 \varepsilon_r \zeta}{\eta \lambda_0} \quad \textbf{(32)}$$

Equation 31 is applied only when there is no overlap of the double layers inside the pores (i.e., when the pore radius and Debye length (κ^{-1}) ratio is large [80]. If the ratio between the pore radius and Debye length is small, then corrections to Equation 31 could prevent an underestimation of membrane's zeta potential.

2.3. Previous Membrane/Colloid Characterization and Fouling Studies

Recently, much attention has been focused on the characterization of membrane surfaces in order to gain an insight into membrane-solute interactions during fouling [6, 55, 81, and 82]. Fewer investigations have characterized both the membrane surface and the potential foulant source (i.e., colloid, NOM, etc.) [6, 81, and 82]. Childress and Deshmukh [1998] [81] used streaming potential measurements to calculate zeta potential for two RO membranes in order to study the effect of solution chemical composition on membrane surface charge and subsequently membrane performance. It was found that both Swannee River humic acid and sodium dodecyl sulfate had a significant influence on salt rejection at low pH where particle adsorption changed membrane zeta potential (from positive to negative) there-by causing a change in co-ion exclusion effects.

A comprehensive approach investigating the adhesion of micro organisms and polystyrene microspheres to membrane surfaces was taken by Meinders et al. [1995] [25]. Meinders et al. [1995] calculated the Lifshitz-van der Waals, electrostatic, and acid-base energies of interaction from measured zeta potentials and contact angles using the XDLVO approach. The adhesion of microorganisms and polystyrene microspheres to several membranes were compared to one another based on their respective interaction energy curves. It was found that the depth of the secondary interaction minimum fully governed the deposition efficiency and the desorption of both the microorganisms and the polystyrene microspheres. Deposition efficiencies increased with increasing depth of the secondary interaction minimum, while desorption decreased with increasing depth.

Zhu and Elimelech [1995] [6] conducted fouling experiments for thin-film composite and cellulose acetate RO membranes using aluminum oxide colloids. The electrokinetic properties of both colloids and membranes were determined using zeta and streaming potential measurements. It was concluded that RO membrane fouling is controlled by colloid-membrane and colloid-retained colloid interactions, which are a function of

solution chemistry (e.g., ionic strength and pH), chemical properties of colloids and membranes, and the magnitude of the permeation drag.

Cho et al. [1998] [82] used several characterization techniques such as contact angle, zeta potential, and infrared (IR) spectra to characterize several commercial nanofiltration (NF) and ultrafiltration (UF) membranes in addition to natural organic matter (NOM) taken from various source waters. Membranes were characterized both before and after fouling had occurred to evaluate differences in hydrophobicity (contact angle), surface charge (zeta potential), and functional groups (IR spectra). Once exposed to the membrane surface the free energy state (hydrophobic or hydrophilic) of the NOM was found to affect that of the exposed membrane. Contact angle increased for membranes fouled hydrophobic NOM and decreased for those fouled with hydrophilic NOM. Furthermore, membranes became more negatively charged (decreasing zeta potential) when exposed to either a hydrophobic or a hydrophilic NOM source. Bhattacharjee et al. [2000] [55] used the surface element integration (SEI) technique to calculate the interaction energy between spheroidal particles and an infinite planar surface. Results were compared to predictions based on Derjaguin's approximation. It was found that the SEI technique more accurately predicted the interaction energy

3. Experimental Process

3.1. RO Membranes

The three RO membranes selected for this investigation were the FT-30, CD, and CE membranes. The FT-30 membrane (Film Tec, Minneapolis, Minnesota) is a thin-film composite polyamide membrane. It is a widely used low-pressure RO membrane made by the interfacial polymerization of 1,3-benzenediamine with trimesoyl chloride [79, 83]. The CD and CE membranes (Osmonics Desal, Vista, California) are heat-treated cellulose triacetate/diacetate blend membranes. All of the membranes were stored in ultrapure water at 5 degrees Celsuis (°C).

3.2. Colloids

Commercial silica (MP-1040) (Nissan Chemical America Corporation, Houston, Texas), aluminum oxide colloids (Aluminum Oxide C) (Degussa Corporation, Akron, Ohio), and polystyrene microspheres (PS02N) (Bangs Laboratories, Inc., Fishers, Indiana) were used as model colloidal foulants. The MP-1040 was supplied dispersed in deionized (DI) water and stored at room temperature in a plastic container supplied by the manufacturer. According to the manufacturer, the MP-1040 has an average particle diameter of 100 nm and a specific gravity of 1.30 at 20˚C [Nissan Chemical Corp. 2000]. The aluminum oxide was supplied as a powder with a BET surface area in the range of 85 to 115 m^2/g,

an average particle diameter of 13 nm, and a density of 3.2 g/cm^3 [Zhu and Elimelech 1995, Degussa 2000]. According to the manufacturer, the Aluminum Oxide C is composed of Al_2O_3 (> 99.6%), Fe_2O_3 (< 0.2%), TiO_2 (< 0.1%) and HCl (< 0.5 %). Polystyrene microspheres (PS02N) (Bangs Laboratories, Inc., Fishers, Indiana) were supplied dispersed in deionized (DI) water (at 10% solids) and stored in a refrigerator at 5˚C. According to the manufacturer, the microspheres have a mean surface area of 3.361×10^{14} μm^2/g, a mean diameter of 20 nm, and a coefficient of variation of approximately 1% for size uniformity.

Colloids tend to bond together to form aggregates thus changing actual particle diameter reported by the manufacturer [6]. Therefore, the size of all three colloids, as reported by the respective manufacturers, was checked using dynamic light scattering measurements [Zeta PALS, Brookhaven Instruments Corp., N.Y.). Dynamic light scattering measures the intensity of light scattered by particles as a function of time [29]. Fluctuations in light intensity, resulting from the Brownian motion of the particles, can be expressed using a correlation function from which the diffusion coefficient of the particles may be directly calculated. Based on the measured diffusion coefficient, an effective hydrodynamic radius of the particles can be calculated according to:

$$a_h = \frac{kT}{6\pi\eta D_\infty} \tag{33}$$

where η is the viscosity of the suspending fluid and D_∞ is the measured diffusion coefficient.

Dynamic light scattering measurements of the sample colloids in a 0.01 M NaCl suspension found the average particle diameter for each colloid to differ from that reported by the manufacturer. The Aluminum Oxide C, PS02N, and MP-1040 colloids had measured diameters of 220.5, 128.2, and 97.9 nm, respectively. Only the MP-1040 colloid had a measured diameter that was close to the diameter reported by the manufacturer (100nm). A previous study (Zhu and Elimelech [1995]) [6] found that the aluminum Oxide C colloids were aggregates composed of primary particles with a diameter of 13 nm, as reported by the manufacturer. It was concluded that the primary particles were bonded irreversibly to form the observed aggregates. This same conclusion was reached for the current investigation. The measured particle diameter for each colloid was that used in all calculations.

3.3. Surface Tension Measurements

3.3.1. Automated Goniometer

The automated goniometer used in this investigation is the Rame-Hart (Mountain Lakes, New Jersey) NRL Contact Angle Goniometer. It is a standard goniometer with image

analysis attachments (i.e., video camera, computer with monitor, and image analysis software). A photograph of the goniometer apparatus is shown in Figure 2.

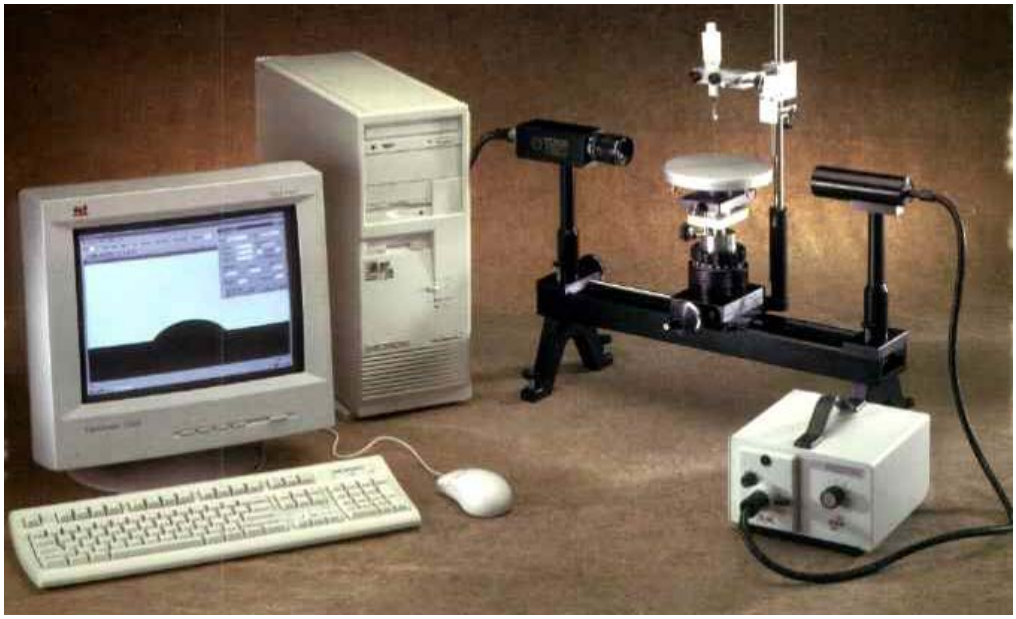

Figure 2. Goniometer apparatus used for contact angle measurements.

The goniometer units (i.e., video camera, light source, and environmental chamber) are built into a metal stand. The stand can be leveled manually with the aid of a leveling bubble and four leveling screws attached to the feet of the stand. This eliminates any slope that may exist in the laboratory test bench that could affect the contact angle measurements. The video camera connects to the computer system through two digital cables. The light source is placed at the opposite end of the video camera. Its intensity is regulated by a control system that is placed on the laboratory bench.

The environmental chamber, used during captive bubble measurements, prevents air movement, dust, and other contaminants from affecting the contact angle measurements or contaminating the probe liquid. The environmental chamber houses a quartz cell, sampling plate, and viewing stage (Figure 3).

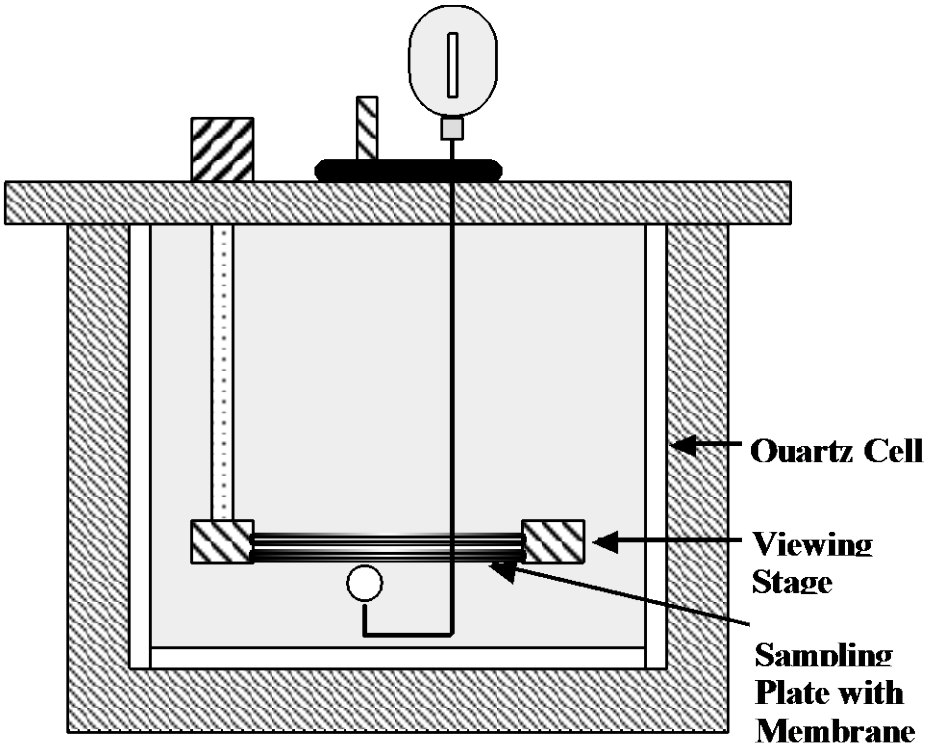

Figure 3. Environmental chamber for captive bubble measurements.

It is constructed of stainless steel and has glass portals on both sides so that the light source and video camera have access to the sampling plate. The sampling plate and viewing stage are also constructed of stainless steel. The sampling plate is secured to the viewing stage using four screws and two cross bars. The viewing stage is lowered into the quartz cell and secured to the top of the environmental chamber with two steel dowels and two tightening screws. A portal is located on the roof of the environmental chamber to allow for insertion of the needle.

The goniometer uses RH Imaging 2001 software, and has both sessile drop and captive bubble capabilities. The image that appears on the computer screen consists of the membrane being viewed by the camera and several lines that are super-imposed by the computer (Figure 4).

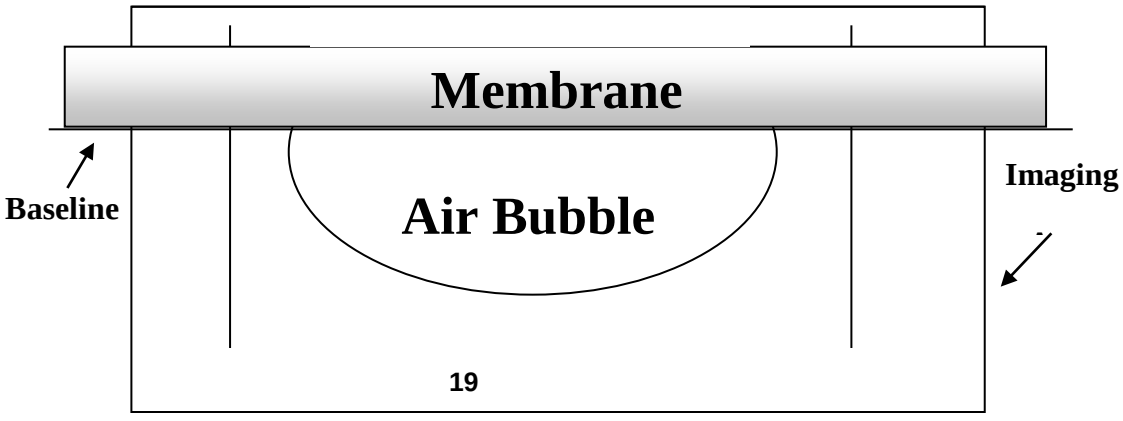

Figure 4. Computer viewing area with the region of interest designated by the superimposed lines.

These lines designate the region of interest and include a rectangular imaging box, a baseline, and two vertical lines. The rectangular imaging box indicates to the computer the area within which contact angle measurements are taken. The size of the rectangular imaging box must be adjusted as the size of the drop or bubble changes. The size of the box should be minimized to only encompass the area of drop or bubble contact to reduce the chance of inaccurate contact angle readings. As the size of the imaging box increases, the possibility of the computer mistaking a surface contaminant for the bubble's point of contact increases. The baseline indicates to the computer where the drop or bubble is contacting the substrate surface and is therefore located at the surface of the substrate. The two vertical lines are gray scale detectors; in other words, they detect the black area (i.e., the substrate) versus the white area (i.e., the probe liquid) of the rectangular imaging box. The two vertical lines must remain half in the black area and half in the white area for proper operation of the imaging software.

To measure contact angles, the computer places a pixel at the point of contact between the bubble or droplet and the substrate surface. Using the pixel as the point of origin, the computer draws a line tangent to the boundary of the bubble. The angle between the tangent line and the baseline is calculated as the contact angle. The contact angle is always measured through the denser fluid phase.

3.3.2. Syringe and U-Shaped Needle

In captive bubble measurements, air bubbles are delivered to the membrane surface using a 10-μl syringe (Hamilton Instruments, Reno, Nevada). The syringe is capable of delivering precise volumes of air (within 0.01 μl) using an attached volume selection and locking mechanism. The ability of the syringe to deliver precise volumes of air reduces errors associated with varying bubble volumes. A bent U-shaped needle is attached to the syringe in order to deliver air bubbles to the underside of the membrane coupon in the environmental chamber. For sessile drop measurements a Gilmont micrometer syringe (Gilmont Instruments, Barrington, Illonois) to deliver liquid drops to the colloidal monolayer. The Gilmont syringe was able to deliver precise liquid volumes within an accuracy of 0.5%.

The needle and syringe are cleaned prior to each set of contact angle measurements. The cleaning procedure utilizes three solvents: ultrapure water, hexane, and acetone. The ultrapure water removes any water-soluble contaminants. The acetone removes any polar but non-water soluble contaminants. The hexane removes any non-polar contaminants. The syringe is cleaned by the following cycle: water, acetone, hexane, water, acetone, hexane, water, water.

3.3.3. Probe Liquids

Surface energy calculations require three probe liquids with well-known surface tension properties [25]. The probe liquids selected for this investigation were ultrapure water

(polar), glycerol (polar), and diiodo methane (apolar). These probe liquids were chosen on the premise that two must be polar and one must be apolar [25]. Ultrapure water was obtained from a Millipore (Burlington, Massachusetts) water purification system. The diiodo methane (Fisher Scientific, Pittsburgh, Pennsylvania) was distilled under a vacuum. The glycerol (Fisher Scientific, Pittsburgh, Pennsylvania) was used without any further purification. Each liquid has three experimentally determined surface tension parameters, γ^{LW}, γ^{+}, and γ^{-}. Various methods have been used to determine the surface energy parameters for the three probe liquids used in this investigation. Therefore, more than one set of surface energy values have been reported for glycerol and diiodo methane. Each set of values were used in calculating surface energy parameters for the membranes and colloids investigated. These parameters as well as the calculated polar energy component, γ^{AB} and the total free energy component, γ^{TOT} are found in Table 1.

Table 1. Surface tension properties (mJ/m2) of probe liquids at 20˚C.

	γ_l^{LW}	γ_l^{+}	γ_l^{-}	γ_l^{AB}	γ_l^{TOT}
Ultrapure Water	21.8	25.5	25.5	51.0	72.8
Glycerol	34.0	3.92	57.4	30.00	64.00
Diiodomethane	50.8	0.0	0.0	0.0	50.8

3.3.4. Bubble Volume

Bubble volume directly affects the contact angle of a liquid on a solid surface [70, 72]. As bubble volume increases, the contact angle reaches a temporary state of equilibrium with the solid surface [74]. The temporary state of equilibrium reached will change based on the amount of available external energy available for overcoming existing energy barriers, such as vibrations or an increase in bubble volume [74]. Therefore, a constant bubble volume must be used to obtain reproducible contact angle results. A 10-µl bubble was selected for this investigation to provide a bubble of significant size to make its edges clearly visible.

3.3.5. Parafilm Standard

Contamination of the contact angle system (i.e., the membrane coupon, quartz cell, syringe, and the probe liquid) must be avoided to obtain correct contact angle measurements [39]. The contamination level of the system, as well as the methodology used in this investigation, was checked by performing contact angle measurements on commercially available Parafilm (Fisher Scientific, Pittsburgh, Pennsylvania) using the captive bubble method. The results were then compared to values from the literature (e.g., Busscher [1983], Good [1973], Dann [1970], Zhang and Hallstrom [1990]) (Table 2). Measurements performed over a three-day period resulted in an average contact angle

of 110 ± 1˚. As can be seen from Table 2, results from this investigation are in complete agreement with those in the literature. Therefore, this system and the cleaning procedures used are adequate for obtaining correct contact angle results.

Table 2. Comparison of contact angle measurements for water on Parafilm.

Current Investigation[1]	Dann [1970][2]	Good [1973][2]	Busscher [1983][1]	Zhang and Hallstrom [1990][1]
110 ± 1˚	110 ± 2˚	110 ± 1˚	108 ± 2˚	108 ± 3˚

[1] Contact angles were measured using the captive bubble technique.

[2] Contact angles were measured using the sessile drop technique.

3.3.6. Contact Angle Measurement Procedure

The procedure used to measure the captive bubble contact angle is outlined below. It should be noted that the set-up of the goniometer and cleaning of the micro-syringe discussed earlier were also part of the procedure.

1. A membrane coupon with the approximate dimensions 1.0 in × 0.25 in was cut from the membrane sample, which had been flushed with ultrapure water under normal operating conditions for a period of 45 hours.

2. The membrane coupon was wrapped around the sampling plate and secured on the viewing stage. The viewing stage was lowered into the probe liquid contained in the quartz cell and the environmental chamber was sealed. The leveling and lighting conditions of the viewing area were checked using the imaging software.

3. A 10-μl air bubble was released from the U-shaped needle into the quartz cell containing the probe liquid. The bubble floated approximately 1.5 cm to the membrane surface held by the viewing stage.

4. The goniometer's video camera was focused on the air bubble.

5. Two contact angle measurements (one on each side of the bubble) were taken at time zero and then at 5-minute intervals over the next 20 minutes.

3.3.7. Colloid Surface Tension

Determination of colloid surface tension through goniometry is similar to the determination of membrane surface energetics in that both utilize goniometry and van

Oss's acid-base approach to calculate surface energies. Several methods have been developed to measure colloidal contact angles. The method of contact angle measurement is typically dependent upon the size of the individual colloids. To measure contact angles for particles with diameters less than 1 μm, as are the three colloids selected for this investigation, the particles must be deposited on a flat surface. The surface may be either porous (membrane) or nonporous (glass slide).

In the current investigation, colloids were deposited onto a nonporous RO membrane using a dead-end membrane filtration system. Contact angle measurements were then performed on the deposited colloid layer using the sessile drop method. Three probe liquids (ultrapure water, glycerol and diiodo methane) were used for the contact angle measurements. The surface properties of the respective colloids were then calculated using the Lifshitz-van der Waals acid-base approach.

The procedure for determining colloid surface energy is summarized in the following steps:

1. A concentrated colloid solution was filtered through a nonporous reverse osmosis (RO) membrane for approximately 24 hours to form a significantly think colloidal layer.

2. The membrane was removed from the membrane filtration system to allow the colloidal layer to dry for 60 minutes.

3. The membrane is secured on the goniometer viewing stage.

4. A 5-μl liquid droplet of ultrapure water, glycerol, or diiodo methane was released from the micrometer syringe at a minimum distance from the colloidal monolayer.

5. The goniometer's video camera was focused on the liquid droplet.

6. Two contact angle measurements (one on each side of the droplet) were taken immediately following deposition of the liquid droplet on the colloidal monolayer.

3.4. Electrokinetic Properties of Membranes and Colloids

3.4.1. 3.4.1. Electrophoretic Mobility of Colloids

The electrophoretic mobility of the Aluminum Oxide C, MP-1040, and PS02N colloids were measured by micro-electrophoresis (Zeta PALS, Brookhaven Instruments Corp., NY). The electrophoretic mobilities of all colloids were measured at three pH values (3.0,

5.6, and 8.0) at an ionic strength of 0.01 M NaCl. The instrument used is comprised of a laser for particle illumination, a monitor for viewing the particles, and a rotating prism. Using the prism, the average mobility of many particles can be determined simultaneously at each measurement. The ability to measure the electrophoretic mobility of several colloids at once was essential for the nanometer-sized colloids used in this investigation.

3.4.2. Streaming Potential of Membranes

Zeta potentials for the RO membranes were determined using a streaming potential analyzer. Commercial reference electrodes were used to measure the streaming potentials along the membrane surfaces and a pair of self-made Ag/AgCl-electrodes were used when measuring streaming potential through the membrane pores. An in-depth description of the cells used may be found elsewhere [84].

Prior to streaming potential analysis, the membranes were cleaned in an ultrasonic bath for three 10-min periods using ultrapure water (conductivity < 1 μS/cm). The water was changed following each period. Before the measurements were conducted, the membranes were pressurized under 2 bar for 1 hour. Streaming potential measurements were conducted in a 1 mM KCl electrolyte solution at 25˚C. Measurements were first conducted in the pure electrolyte solution (pH 5.4 ~ 5.8) without any pH adjustment. The pH of the electrolyte solution was then made more acidic through the titration of 1.0 M HCl. The streaming potential was measured at five different pressure differentials for each pH value. Measurements were begun at the highest-pressure differential before being gradually lowered. The flow velocity through the cell was maintained at 0.5 m/s in order to sustain laminar flow conditions. Pressure gradients over the flow channel between the two membrane coupons were generated by changing the speed of the gear pump when measuring along the surface. Zeta potentials were calculated from the streaming potential results using the Helmholtz-Smoluchowski equation (Equation 34) [80]:

$$\zeta = \frac{\Delta E_s \kappa \mu}{\Delta p \varepsilon_0 \varepsilon_1} \quad \textbf{(34)}$$

where ζ is the zeta potential, ΔE_s is the induced potential difference between the electrodes (streaming potential), Δp is the applied pressure, ε_0 is the permittivity in a vacuum, ε_1 is the dielectric constant of the electrolyte solution, κ is the conductivity of the electrolyte solution, and μ is the viscosity of the electrolyte solution.

3.5. Membrane Performance Tests

3.5.1. Membrane Test Unit

The membrane test unit used in this investigation was a bench-scale RO/NF system with fully automated data acquisition. It is capable of operation in constant flux (J) or constant pressure (ΔP_{TM}) modes. Constant flux or transmembrane pressure was achieved by manipulating the permeate back-pressure using a needle valve. For constant flux operation, the permeate needle valve would be opened as pressure increased with fouling. Constant pressure operation was achieved by either opening or closing the permeate needle valve based on changes in flux. During typical runs, the permeate needle valve was slowly closed as the permeate flow decreased with membrane fouling. The membrane test unit was operated in a cross-flow flow configuration because this configuration is more advantageous when removing colloids from a process stream [11]. In-line computer interfaced digital probes (Cole Parmer Instrument Company, Vernon Hills, Illinois) were used to measure temperature, pH, conductivity, flowrate, and pressure. Data was acquired and displayed by LabVIEW data acquisition software (National Instruments, Austin, Texas). LabVIEW uses the probes as virtual instruments that may be controlled and viewed using a central computer.

A schematic of the membrane test unit is shown in Figure 5.

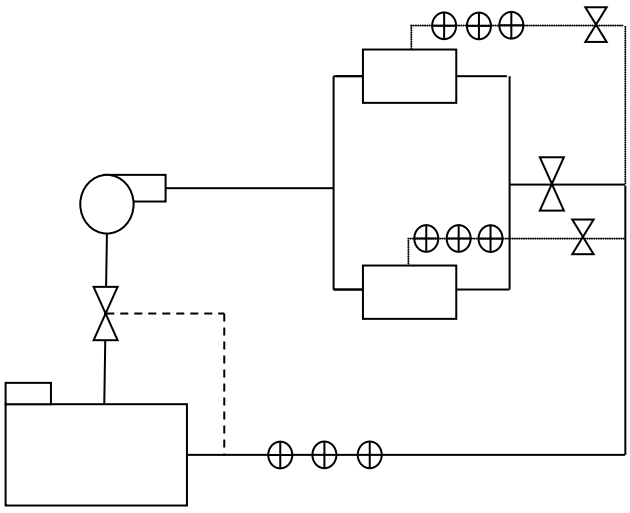

Figure 5. Bench scale membrane test unit.

The test solution was held in a 28-L refrigerated bath (Cole-Parmer, Vernon Hills, Illinois). Bath temperature was maintained at 20 C by using the digital temperature control feature on the bath unit. The test solution was fed to two parallel flat sheet

membrane test cells (Industrial Research Machine Products Co., Los Angles, California) using a positive displacement pump (CAT Model 280, Aries Supply and Equipment Company, North Hollywood, California) capable of providing hydraulic pressures up to 1000 psi and a maximum flowrate of 3 gpm. The two membrane test cells operated at a constant cross-flow velocity of 3.22 ft/sec for all trials. The test cells contained flat sheet membrane coupons with dimensions of 1.0 in × 3.0 in, for an active membrane area of 3.0 in^2. Both permeate and concentrate streams were recycled to the reservoir. Pressure across the membrane cells was controlled using a back-pressure regulator (Oakland Valve and Fittings, Concord, California) located on the concentrate return line.

Feed solution conductivity and pH were measured using in-line computer-interfaced probes. Transmembrane pressure was measured using computer-interfaced in-line pressure transducers located on both the influent and effluent sides of the membrane test cells. The pressure transducers can measure pressures ranging from 0 to 1000 psi with a reported accuracy of 0.5%. Both feed and permeate flowrates were measured using in-line flow meters (Alicat Scientific Precision Liquid Flowmeter). Ion rejection and permeate pH were measured using in-line conductivity and pH probes, respectively.

3.5.2. Solution Chemistries

Four test solutions were used in the membrane performance test:

1) 0.01 M NaCl

2) MP-1040 colloids plus 0.01 M NaCl

3) Aluminum Oxide C colloids plus 0.01 M NaCl.

4) PS02N plus 0.01 M NaCl

Certified ACS grade sodium chloride (0.01 M NaCl) (Fisher Scientific, Pittsburgh, Pennsylvania) was used for the baseline. Then, 0.01 M NaCl was used as a background electrolyte for the colloidal fouling studies. As ionic strength increases colloidal stability decreases due to compression of the colloidal EDL, thus decreasing double layer repulsion [6]. However, at low ionic strengths (e.g., ≤ 0.01 M NaCl) colloidal particles are relatively stable due to strong interparticle electrostatic repulsion. Therefore a relatively low ionic strength (i.e., 0.01 M NaCl) was used to minimize the colloids from coagulating and forming large particles. An ionic strength of 0.01 M NaCl has been shown to be an acceptable ionic strength for preserving colloid stability in studies using similar colloids as model foulants [11]. Colloid suspensions were prepared by adding a known amount of colloid stock solution to DI water followed by intense mixing for 30-min and then ultrasonication for an additional 30-minutes prior to addition to the test solution. Intense mixing and ultrasonication prevents the colloids from forming large aggregates before introduction into the feed-stream.

3.5.3. Performance Test Protocol

Prior to the performance test, the membrane coupons were rinsed in a flow through mode with 5.5 gal of ultrapure water to remove impurities that may be attached to the membrane surface. The membranes were then equilibrated under normal operating pressure for approximately 45 hrs with 0.01 M NaCl solution. As long as the permeate flux and salt rejection were found to be constant, the experiment was continued. The colloids were added to the feed solution immediately following the 45-hr equilibration period. Because colloid transport to the membrane surface is a function of flux, the initial flux for all membranes were made identical by manipulating permeate back-pressure as described earlier. It is essential that the different membranes operate under the same initial flux in order to accurately draw correlations between the respective fouling rates and surface parameters by eliminating differences in permeation drag [Zhu and Elimelech 1997] [53].

Membrane performance tests were conducted for a period of approximately 3 hours after the 45-hour equilibration period. Membrane performance was evaluated at pH ~ 5.6. The flux and rejection of each membrane was monitored at 10-min intervals over the 3-hour observation period. Hydrodynamic conditions for all three membranes (CE, CD, and FT-30) remained constant. Experiments were conducted at a constant transmembrane pressure of 425 psi for the cellulose acetate membranes (CE and CD) and 225 psi for the thin-film composite membrane (FT-30). Transmembrane pressures for both cellulose acetate and thin-film composite membranes were based on the manufacture's recommended operating pressure.

3.5.4. Performance Analysis

The effect of the colloids on membrane performance were quantified using flux and rejection ratios. Flux and rejection ratios provide a method for comparing changes in flux and rejection for membranes that have a wide range of initial flux or rejection values [41]. The flux ratio is a ratio of the water flux at time, t, to the original water flux prior to the addition of the foulant. The flux ratio was calculated using Equation 35:

$$J_i = \frac{j_i}{j_0} \tag{35}$$

where J_I is the flux ratio at time t, j_I is the water flux at time t, and j_o is the original water flux prior to addition of the colloidal foulant. The times evaluated in this investigation were 5 min, 20 min, 35 min, and 50 min after the addition of the foulant. These times correspond to j_5, j_{20}, j_{35}, and j_{50} in Figure 10. Similarly, rejection ratios were calculated at 5 min, 20 min, 35 min, and 50 min using Equation 36:

$$R_i = \frac{r_i}{r_o} \tag{36}$$

where R_I is the rejection ratio at time t, r_I is the salt rejection at time t, and r_o is the original salt rejection prior to addition of the colloidal foulant.

4. Results and Discussion

4.1. Surface Energy Calculations

Average contact angle measurements for the probe liquids on the three membranes (FT-30, CD, and CE) and the three colloids (silica, alumina, and polystyrene) are shown in Table 3. The values in Table 3 for the membranes represent the mean of at least 18 air bubbles, and are reported with their respective 95% confidence limits. The membrane contact angle measurements were highly reproducible for all membrane-probe liquid combinations investigated with 95% confidence limits of less than 3°. The values for the silica and alumina colloids are reported as the mean of three air bubbles.

Table 3. Average contact angle measurements for membranes and colloids investigated.

	Ultrapure Water	Glycerol	Diiodomethane
Membranes			
FT-30	49° (± 0.8°)	47° (± 1.0°)	54° (± 0.6°)
CE	45° (± 2.1°)	41° (± 1.6°)	44° (± 1.4°)
CD	49° (± 1.2°)	58° (± 1.5°)	43° (± 2.4°)
Colloids			
Silica	67°	80°	50°
Alumina	44°	23°	33°
	Ultrapure Water	Formamide	Diiodomethane
Polystyrene*	90°	74°	44°

* Data taken from Busscher et al. 1984 [85].

Table 4 shows the calculated surface tension parameters and the free energy of cohesion for each of the membranes and colloids. The surface energy data show that all three membranes have high electron donor monopolarity, or high electron donor components (γ^-) and relatively low electron acceptor components (γ^+). These results agree with previous studies (e.g., [4 and 34]) that have found that polymeric membranes are typically characterized by a high electron donor monopolarity. Specifically, the CD membrane has an especially low electron acceptor component, which translates into a very low AB component. Furthermore, the CD membrane is strongly hydrophilic while

the FT-30 and CE membranes cannot be said to be hydrophobic or hydrophilic with ΔG_{sws} approximately equal to zero. Similar to the membranes, the colloids are characterized as having high electron donor monopolarity. The silica colloid is hydrophilic while the alumina and polystyrene colloids are hydrophobic.

The free energy of cohesion is the interaction free energy (per unit area) when two surfaces of the same material are immersed in a solvent (in this case, water) and brought into contact. These values provide a quantitative insight regarding the hydrophobicity/hydrophilicity of the membranes and colloids. Positive values of the cohesive energy imply hydrophilic surfaces, while negative values indicate hydrophobic surfaces. The free energy of cohesion may provide some qualitative insight into potential interactions between membranes and colloids. For example, based on the values given in Table 4, the short range interaction between the CD membrane and silica colloid may be considered to be strongly hydrophilic and therefore, repulsive. However, in many cases, cohesive energies may also provide misleading notions about the interaction between membranes and colloids, primarily due to its inability to provide a quantitative assessment of adhesive energies between the membrane and colloid. Free energies of cohesion are discussed in relation to free energies of adhesion in Section 4.3.

Table 4. Surface energy parameters (mJ/m^2) for membranes and colloids calculated from contact angle measurements.

	γ^{LW}	γ^+	γ^-	γ^{AB}	γ^{TOT}	ΔG_{sws}
Membranes						
FT-30	32.02	1.76	29.12	14.34	46.35	2.57
CE	37.44	1.69	28.60	13.90	51.34	16.58
CD	38.12	0.025	36.38	1.92	40.04	0.10
Colloids						
Silica	34.27	3.58	35.37	22.51	56.78	6.57
Alumina	42.94	3.72	19.42	17.00	59.94	-14.97
Polystyrene	37.54	0.57	5.27	3.47	41.00	-51.60

4.2. Zeta Potential Determination

The pH dependence of the zeta potentials for the three membranes is shown in Figure 6. For the CD membrane, the potential is positive in the lower pH range, passes through an isoelectric point around pH 4, and then becomes negative in the higher pH range. The CE and FT-30 membranes are negatively charged over the entire pH range investigated.

Detailed descriptions of the mechanisms controlling the surface charge of thin-film composite and cellulose acetate membranes were presented in earlier publications (e.g., [79, 86]). The membrane zeta potential curves were determined using a background electrolyte of 1 mM KCl. A notable feature regarding the charge behavior of the membranes that becomes evident when Figure 6 is compared to Figure 7 is that all the membranes have very small zeta potentials (< 10 mV). Because the zeta potentials of the membranes are expected to vary only minimally with ionic strength [79], the measured values of zeta potential were employed in calculations of DLVO and XDLVO interactions that assume a background electrolyte of 10 mM NaCl.

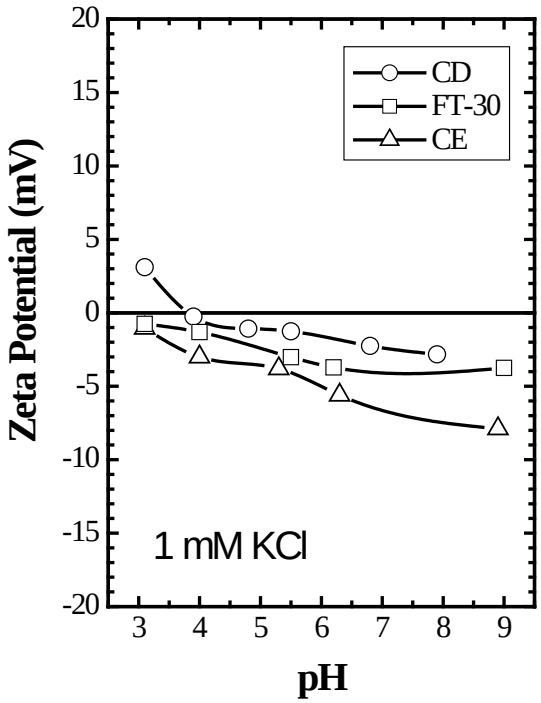

Figure 6. Variation of the zeta potential of membranes with pH. Measurements were carried out with a background electrolyte of 1 mM KCl.

Zeta potential curves for the three colloids as a function of pH are presented in Figure 7. With an isoelectric point of approximately 7.5, the alumina colloids are positively charged over the majority of the pH range studied. The silica and polystyrene colloids are negatively charged over the entire pH range investigated. In sharp contrast with the membranes, the zeta potentials of the colloidal particles were found to be substantially larger in magnitude over certain pH ranges. Therefore, electrostatic double layer interactions between the membranes and colloids involve highly asymmetric surfaces with very different potentials.

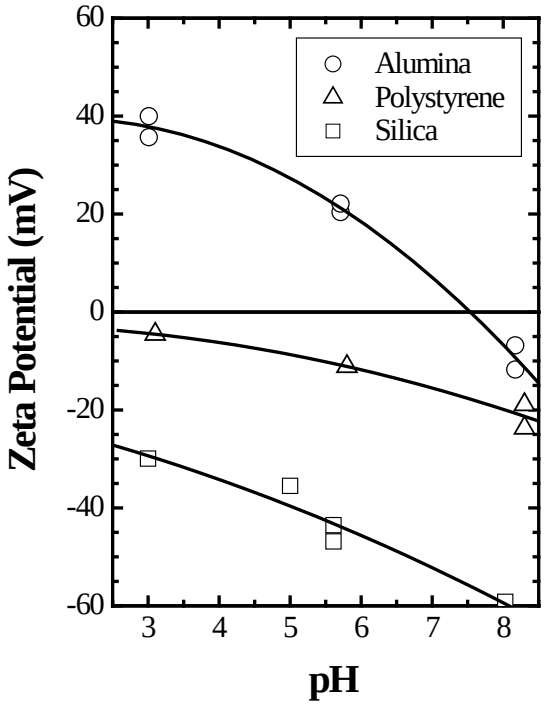

Figure 7. Zeta potential of colloids as a function of pH. Measurements were carried out with a background electrolyte of 10 mM NaCl.

4.3. Interaction Energy at Contact

Table 5 shows DLVO and XDLVO predictions of the free energy of adhesion per unit area for the various membrane-colloid pairs tested. These values were calculated using Equations. 20, 21, and 28. In Equation 28, the minimum separation distance of 0.158 nm was used.

The DLVO theory predicts a weak attraction for all of the membrane-colloid combinations with all interaction energies ranging from approximately -3 to -7 mJ/m^2. Even though both the membranes and colloids (except for alumina) are negatively charged, the DLVO theory (based on constant potential EL interactions) predicts mild attraction because the membranes have very low surface potentials compared to the colloids. In general, when the constant potential assumption is used, highly asymmetric surfaces are mildly attractive; however, if constant charge is assumed, this may not be the case [87].

Table 5. Interaction energy at contact (mJ/m^2) for membranes and colloids calculated from DLVO and XDLVO theories.

	Silica	Alumina	Polystyrene
DLVO			
FT-30	-5.63	-5.18	-2.98
CD	-7.16	-6.90	-4.53
CE	-6.56	-7.06	-4.31
XDLVO			
FT-30	1.14	-7.91	-20.74
CD	7.20	-6.40	-22.54
CE	0.14	-9.95	-22.48

The XDLVO predictions show that including AB interactions results in a substantially different prediction for the free energy of adhesion for several of the membrane-colloid combinations. In the case of the silica colloid, the XDLVO predictions show a repulsive interaction at contact with all of the membranes, which is qualitatively different from the predictions of the DLVO theory. Specifically, a complete reversal of the free energy of adhesion (from -7.2 mJ/m^2 to +7.2 mJ/m^2) is observed for the CD-silica combination. In the case of the polystyrene colloid, XDLVO predictions show a much stronger attraction than was predicted by the DLVO theory. The large negative value of the free energy of adhesion for the polystyrene colloid based on the XDLVO approach corroborates the strongly hydrophobic nature of this colloid. The substantial differences between DLVO and XDLVO predictions imply that the fouling predictions for the membranes and colloids would be completely different if the AB component is ignored.

It is important to note the differences between the free energy of adhesion results for each membrane-colloid combination (Table 5) and the free energy of cohesion results for the individual membranes and colloids (Table 4). For example, according to the cohesion results, all of the membranes would be expected to have low fouling tendencies because the free energies of cohesion are positive. However, when the free energies of adhesion for the different membrane-colloid combinations are considered, a more comprehensive picture of the fouling tendency is developed. The CD membrane, which is expected to have the lowest fouling tendencies according to the free energy of cohesion values, actually does not exhibit a substantially different fouling tendency than the other membranes when exposed to alumina or polystyrene.

It was stated earlier that the presence of additional interactions (such as polar interactions) is just one possible mechanism to explain deviations from DLVO theory. A second plausible mechanism is surface roughness [10]. In this context, the results from Table 5 give considerable insight into the relative importance of morphological heterogeneity and polar interactions on the deviation of the total membrane-colloid interaction energy from the DLVO prediction. Because the membrane-colloid interaction energy dictates the initial fouling behavior, careful analysis of the surface energies from Table 5 may be used to delineate the conditions under which roughness alone cannot explain aberrant fouling tendencies.

Earlier studies dealing with the influence of roughness on DLVO interactions have found that roughness primarily brings the surface energies closer to zero (reduces the magnitude of the interaction). More specifically, calculations for interaction energies between rough surfaces near contact reveal that electrostatic and van der Waals interactions are considerably lower than they are for corresponding smooth surfaces [20, 21]. The presence of roughness alone can never induce a complete reversal of the interaction energy, or more specifically, render the interaction repulsive. The CD-silica adhesive energies in the current investigation, however, change from -7 mJ/m^2 to +7 mJ/m^2 (see Table 5) in the presence of AB interactions. Such an enhanced repulsion could never be solely attributed to surface roughness. Hence, the fouling behavior of CD membranes in the presence of silica could not have been explained by roughness alone. Careful analysis of the surface energetics can thus provide considerable insight into the relative importance of polar interactions and physical heterogeneity on the membrane-colloid interactions. In order to gain a comprehensive insight into membrane fouling, it is therefore advisable to simultaneously assess the effects of roughness and polar interactions (surface energetics).

4.4. DLVO and XDLVO Energy Profiles for Membrane-Colloid Systems

Figure 8 shows DLVO and XDLVO interaction energy profiles for the nine membrane-colloid systems. For each membrane-colloid combination, Equations. 25, 27 and 29 were used to calculate the LW, EL, and AB components of the interaction energies. These components were then added together according to either Equation 1 or Equation 2 to obtain the DLVO or XDLVO energy, respectively. The horizontal axis (separation distance) is plotted using a logarithmic scale to emphasize the substantial short-range differences between the DLVO and XDLVO predictions. It can be noted from Figure 8 that deviations between the DLVO and XDLVO predictions disappear at larger separations (> 5 nm).

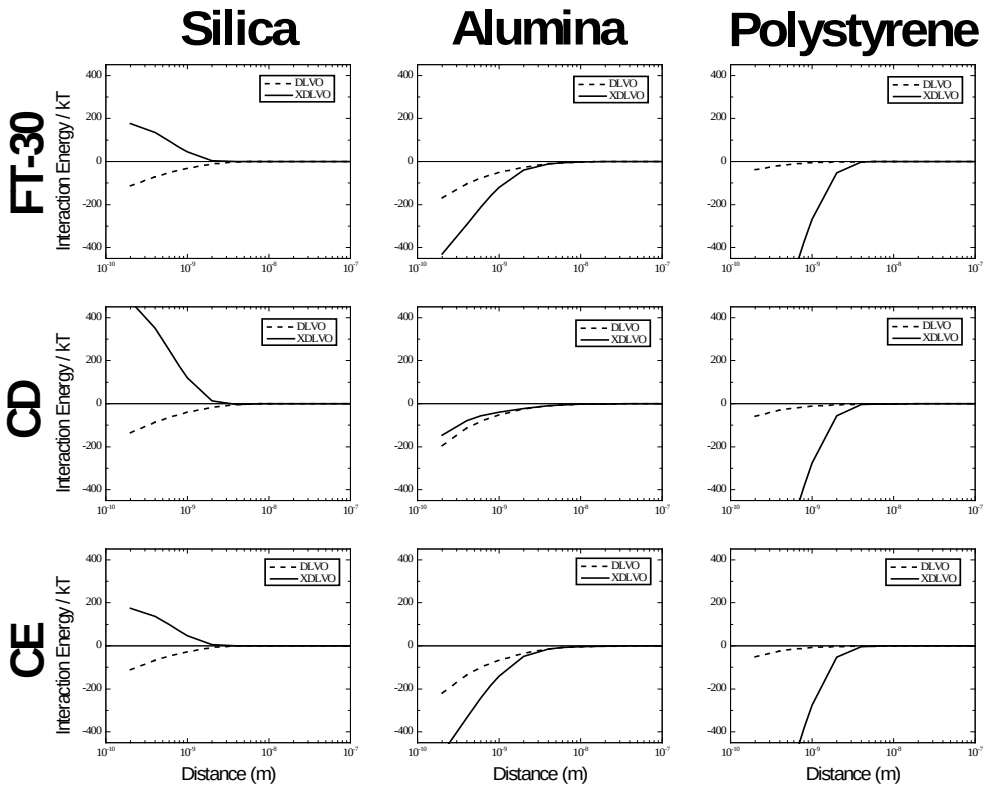

Figure 8. DLVO and XDLVO interaction energy profiles for all membrane-colloid combinations tested (I = 0.01 M NaCl); pH = 5.6). The rows designate the type of membrane, while the columns correspond to the different colloids. Values for interaction energy at contact were taken from Table 5.

The first observation that can be made is that the behavior of the membrane-colloid system is generally controlled by the colloid surface energetics. In other words, no matter what membrane the colloid is paired with, the DLVO and XDLVO curves are quite similar for each colloid. The primary reason for this behavior is the considerably higher surface energies of the colloids compared to the membranes. The exception to this is the CD-alumina system, which has different DLVO and XDLVO interactions than the FT-30-alumina and CE-alumina systems.

For the silica colloid, the XDLVO approach predicts repulsion while the DLVO theory predicts attraction. For each membrane-silica combination, the AB interaction component is repulsive due to the hydrophilic nature of the silica colloid (ΔG_{sws} = 6.57 mJ/m^2). In the case of the polystyrene colloid, the XDLVO approach predicts much stronger attraction than the DLVO theory. In the membrane-polystyrene systems, the AB interaction component is attractive due to the highly hydrophobic nature of the polystyrene colloid (ΔG_{sws} = -51.60 mJ/m^2). The FT-30-alumina and CE-alumina systems behave similarly to their polystyrene counterparts. The attractive AB interaction component results in the XDLVO approach predicting stronger attraction than the DLVO theory. However, in the

case of the CD-alumina system, the high surface energy of the CD membrane results in a repulsive AB interaction. Unlike the polystyrene system where the strong hydrophobicity of the colloid overcame the hydrophilic tendency of the CD membrane, the less strong hydrophobicity of the alumina colloid doesn't overcome the hydrophilic tendency of the CD membrane. Therefore, for the CD-alumina system, the XDLVO prediction does not substantially deviate from the DLVO prediction.

On the basis of the above interaction energy profiles, it is fairly straightforward to assess the fouling tendencies of a given membrane in the presence of different colloids. For the membranes, colloids, and solution chemistry in this investigation, the hydrophilic silica colloid would be expected to foul a membrane to a lesser degree than the strongly hydrophobic polystyrene colloids. It should be noted that this difference between silica and polystyrene is not predicted by the DLVO potentials, which predicts similar fouling propensities for both colloids.

4.5. Implications of DLVO and XDLVO Energy Profiles for Membrane Fouling

Initial attachment of colloids to the membrane surface is controlled by adhesive energies between the colloids and the membrane surfaces. Over time, a membrane surface eventually becomes covered with colloids, and consequently, the interaction energy between approaching colloids and deposited colloids will govern additional fouling. At this time, fouling tendencies will be controlled by the energy of cohesion between approaching and deposited colloids rather than the energy of adhesion between approaching colloids and the membrane surface. Figure 9 shows DLVO and XDLVO interaction energy profiles for each colloid-colloid system.

Equations 25, 27 and 29 were again used to calculate the LW, EL, and AB components of the interaction energies. However, the surface tension characteristics of the membrane surface were replaced with colloid surface tension characteristics. The resulting components were then added together according to either Equation 1 or Equation 2 to obtain the DLVO or XDLVO energy, respectively. It is important to note that electrostatic interactions become very important in cohesive interactions because the interaction is occurring between two surfaces with the same potential. The result, which can be seen by comparing Figures 8 and 9, is strong electrostatic repulsion that causes a more repulsive DLVO interaction.

The DLVO and XDLVO predictions of polystyrene-polystyrene interaction energies are similar to the polystyrene-membrane DLVO and XDLVO predictions. This provides further evidence that the strong hydrophobicity of the polystyrene colloid (see Table 4) dominates interactions involving this colloid and results in strong attractive energies. The DLVO and XDLVO predictions of alumina-alumina interaction energies show that approaching colloids will be attracted to deposited colloids in generally the same manner as the approaching colloids are attracted to the membrane surface. The most significant exception to this is the case of the CD-alumina system where the hydrophilicity of the

CD membrane causes the XDLVO approach to predict a weaker attraction than the DLVO theory. Whereas in the alumina-alumina system, because the membrane surface energetics no longer play a role, the XDLVO approach predicts a stronger attraction than the DLVO theory. Unlike the polystyrene and alumina profiles, DLVO and XDLVO predication of silica-silica interaction energies show that approaching silica colloids experience repulsion to the deposited silica colloids. Whereas in all of the membrane-silica cases where DLVO predictions are attractive and XDLVO predictions are repulsive, in the silica-silica case, the DLVO prediction is weak repulsion and the XDLVO prediction is a much stronger repulsion. The DLVO prediction of weak repulsion is due to strong electrostatic repulsion caused by the high negative potential of the silica colloid (see Figure 7). The XDLVO prediction of strong repulsion in silica-silica interactions is due to the hydrophilicity of the silica colloid (see Table 4).

Based on the XDLVO predictions of repulsion between the silica colloid and the membrane surface and between approaching silica colloids and deposited silica colloids, the silica colloids would be expected to have less propensity towards forming a thick fouling layer than either the alumina or polystyrene colloids. Based on the strong adhesion forces predicted between the membranes and the polystyrene colloids and the strong cohesion forces predicted among the polystyrene colloids themselves, the polystyrene colloids would be expected to form a very thick fouling layer. However, it is important to note that how the energetics change with time will also depend on a variety of physicochemical parameters such as particle concentration, applied pressure (which governs the permeation drag), crossflow velocity, and electrolyte concentration.

4.6. Fouling Results

Figure 10 shows the flux decline behavior for the FT-30 membrane in the presence of the silica, alumina, and polystyrene colloids. The normalized permeate flux following the addition of colloids to the feed stream is plotted as a function of time. Substantial differences exist in the lag time before losses of permeate flux were observed for each of the three colloids. For the polystyrene colloid, there was a lag time of approximately 1.2 hrs before loss of permeate flux was observed; for the alumina colloid there was a lag time of approximately 1.7 hours; and for the silica colloid there was a lag time of approximately 3 hours.

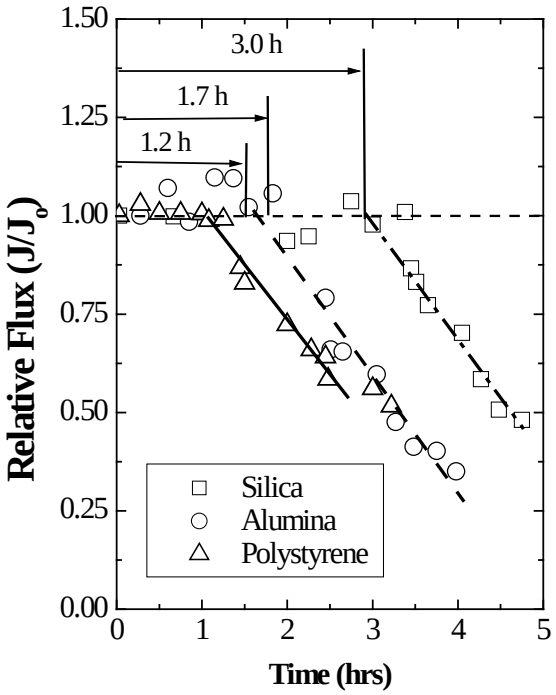

Figure 10. Normalized permeate flux as a function of time following colloid addition to the feed stream for the FT-30 membrane and the three colloid solutions (colloid concentration = 1.37 x 1015 colloids/L; I = 0.01 M NaCl; pH = 5.6).

As RO membranes intrinsically have large resistance to water flux, a loss of permeate flux will only be observed once a sufficiently thick cake layer has formed on the membrane surface. In the earliest stages, interactions between the colloids and membrane will occur. However, it is likely the interactions between the approaching and deposited colloids that will ultimately control the rate of cake layer growth, and hence the lag time before permeate flux loss is seen.

Based on the XDLVO predictions for both membrane-colloid and colloid-colloid interactions, the polystyrene colloid was expected to have the greatest fouling propensity and the silica colloid was expected to have the least. Indeed, this fouling trend is observed in Figure 10 where the lag time for the silica colloid is much higher than that for the polystyrene colloid. And although these results are not a quantitative assessment, they provide promising evidence as to the significance of polar interactions on colloidal membrane fouling.

5. Conclusions

A comprehensive analysis of membrane and colloid surface energetics is a prerequisite for understanding the influence of polar (hydrophobic/hydrophilic) interactions on colloidal membrane fouling. It is demonstrated that specifying the surface energies of a membrane alone does not necessarily indicate whether a membrane will be fouling resistant. Rather, it is necessary to assess the adhesive energy between the membrane and the colloid to predict the fouling behavior. With this understanding, it seems pertinent to focus on means for minimizing colloid-membrane and colloid-colloid adhesive energies during membrane filtration processes instead of focusing attention only on manufacturing "low-energy membranes" and disregarding the interfacial properties of the foulants.

The XDLVO approach (which considers AB interactions) predicts substantially different interaction energies for several of the membrane-colloid combinations investigated compared to DLVO predictions. Strongly hydrophilic systems (e.g., the silica-membrane combinations) demonstrate that the monotonic attraction predicted by the DLVO theory may become repulsion when analyzed using the XDLVO approach. On the other hand, in strongly hydrophobic systems (e.g., any of the polystyrene systems), the weak DLVO attraction may be significantly magnified due to the additional hydrophobic attraction. On the basis of the DLVO theory, all of the membrane-colloid combinations were predicted to have a weak attraction, and hence, similar fouling tendencies. However, when the AB interactions are considered in the XDLVO approach, there is a marked difference in the total interaction energies. This suggests, for example, that the fouling behavior of silica will be substantially different from the fouling behavior of polystyrene. Furthermore, based on colloid-colloid surface energetics, the rate of fouling due to silica-silica interactions was predicted to be substantially lower than the rate of fouling due to polystyrene- polystyrene interactions. The higher propensity of fouling for the polystyrene colloids versus that for the silica colloids was supported by preliminary fouling results for the FT-30 membrane and three colloidal solutions.

References

[1] M. Nyström, L. Kaipia and S. Luque, Fouling and retention of nanofiltration membranes, Journal of Membrane Science 98 (1995) 249.

[2] K.J. Kim, V. Chen and A.G. Fane, Ultrafiltration of colloidal silver particles: flux, rejection, and fouling, Journal of Colloid and Interface Science 155 (1993) 347.

[3] S. Bhattacharjee, A. Sharma and P.K. Bhattacharya, Surface interactions in osmotic pressure controlled flux decline during ultrafiltration, Langmuir 10 (1994) 4710.

[4] L. Gourley, M. Britten, S.F. Gauthier and Y. Pouliot, Characterization of adsorptive fouling on ultrafiltration membranes by peptides mixtures using contact angle measurements, Journal of Membrane Science 97 (1994) 283.

[5] M. Elimelech, J. Gregory, X. Jia and R.A. Williams, Particle Deposition and Aggregation: Measurement, Modelling, and Simulation, Butterworth-Heinemann, Oxford, 1995.

[6] X. Zhu and M. Elimelech, Fouling of reverse osmosis membranes by aluminum oxide colloids, Journal of Environmental Engineering 121 (1995) 884.

[7] A.-S. Jönsson and B. Jönsson, Ultrafiltration of colloidal dispersions - a theoretical model of the concentration polarization phenomena, Journal of Colloid and Interface Science 180 (1996) 504.

[8] L. Meagher, C. Klauber and R.M. Pashley, The influence of surface forces on the fouling of polypropylene microfiltration membranes, Colloids and Surfaces A: Physicochemical and Engineering Aspects 106 (1996) 63.

[9] J.A. Nilson and F.A. DiGiano, Influence of NOM composition on nanofiltration, Journal of American Water Works Association 88 (1996) 53.

[10] M. Elimelech, X. Zhu, A.E. Childress and S. Hong, Role of membrane surface morphology in colloidal fouling of cellulose acetate and composite aromatic polyamide reverse osmosis membranes, Journal of Membrane Science 127 (1997) 101.

[11] S. Hong and M. Elimelech, Chemical and physical aspects of natural organic matter (NOM) fouling of nanofiltration membranes, Journal of Membrane Science 132 (1997) 159.

[12] R.S. Faibish, M. Elimelech and Y. Cohen, Effect of interparticle electrostatic double layer interactions on permeate flux decline in crossflow membrane filtration of colloidal suspensions: an experimental investigation, Journal of Colloid and Interface Science 204 (1998) 77.

[13] S.G. Yiantsios and A.J. Karabelas, The effect of colloid stability on membrane fouling, Desalination 118 (1998) 143.

[14] A.R. Roudman and F.A. DiGiano, Surface energy of experimental and commercial nanofiltration membranes: effects of wetting and natural organic matter fouling, Journal of Membrane Science 175 (2000) 61.

[15] M. Zhang and L. Song, Mechanisms and parameters affecting flux decline in cross-flow microfiltration and ultrafiltration of colloids, Environmental Science and Technology 34 (2000) 3767.

[16] E.M. Vrijenhoek, S. Hong and M. Elimelech, Influence of membrane surface properties on initial rate of colloidal fouling of reverse osmosis and nanofiltration membranes, Journal of Membrane Science 188 (2001) 115.

[17] E.J.W. Verwey and J.T.G. Overbeek, Theory of the Stability of Lyophobic Colloids, Elsevier, Amsterdam, 1948.

[18] S. Bhattacharjee, A. Sharma and P.K. Bhattacharya, Estimation and influence of long range solute. Membrane interactions in ultrafiltration, Industrial and Engineering Chemistry Research 35 (1996) 3108.

[19] M. Elimelech and C.R. O'Melia, Effect of electrolyte type on the electrophoretic mobility of polystyrene latex colloids, Colloids and Surfaces 44 (1990) 165.

[20] S. Bhattacharjee, C.-H. Ko and M. Elimelech, DLVO interaction between rough surfaces, Langmuir 14 (1998) 3365.

[21] J.Y. Walz, The effect of surface heterogeneities on colloidal forces, Advances in Colloid and Interface Science 74 (1998) 119.

[22] Z. Adamczyk and P. Weronski, Application of the DLVO theory for particle deposition problems, Advances in Colloid and Interface Science 83 (1999) 137.

[23] K. Cooper, N. Ohler, A. Gupta and S. Beaudoin, Analysis of contact interactions between a rough deformable colloid and a smooth substrate, Journal of Colloid and Interface Science 222 (2000) 63.

[24] J.A. Molina-Bolivar, F. Galisteo-Gonzalez and R. Hidalgo-Alvarez, The role played by hydration forces in the stability of protein-coated particles: non-classical DLVO behavior, Colloids and Surfaces B: Biointerfaces 14 (1999) 3.

[25] C.J. van Oss, Acid-base interfacial interactions in aqueous media, Colloids and Surfaces A 78 (1993) 1.

[26] H. Yotsumoto and R.-H. Yoon, Application of extended DLVO theory, Journal of Colloid and Interface Science 157 (1993) 434.

[27] A. Grabbe and R.G. Horn, Double-layer and hydration forces measured between silica sheets subjected to various surface treatments, Journal of Colloid and Interface Science 157 (1993) 375.

[28] R.-H. Yoon and S.A. Ravishankar, Application of extended DLVO theory III. Effect of octanol on the long-range hydrophobic forces between dodeclyamine-coated mica surfaces, Journal of Colloid and Interface Science 166 (1994) 215.

[29] J.M. Meinders, H.C. van der Mei and H.J. Busschre, Deposition efficiency and reversibility of bacterial adhesion under flow, Journal of Colloid and Interface Science 176 (1995) 329.

[30] R. Bos and H.J. Busscher, Role of acid-base interactions on the adhesion of oral strepococci and actinomyces to hexadecane and chloroform - influence of divalent cations and comparison between free energies of partitioning and free energies

obtained by extended DLVO analysis, Colloids and Surfaces B: Biointerfaces 14 (1999) 169.

[31] W. Wu, R.F. Giese and C.J. van Oss, Stability versus flocculation of particle suspensions in water - correlation with the extended DLVO approach for aqueous systems, compared with classical DLVO theory, Colloids and Surfaces B: Biointerfaces 14 (1999) 47.

[32] S. Bhattacharjee and A. Sharma, Apolar, polar, and electrostatic interactions of spherical particles in cylindrical pores, Journal of Colloid and Interface Science 187 (1997) 83.

[33] I. Nezbeda, On the role of short- and long-range forces in aqueous systems, Journal of Molecular Liquids 85 (2000) 249.

[34] C.R. Bouchard, J. Jolicoeur, P. Kouadio and M. Britten, Study of humic acid adsorption on nanofiltration membranes by contact angle measurements, The Canadian Journal of Chemical Engineering 75 (1997) 339.

[35] S. Ohki and H. Ohshima, Interaction and aggregation of lipid vesicles (DLVO theory versus modified DLVO theory), Colloids and Surfaces B: Biointerfaces 14 (1999) 27.

[36] R.J. Good, Contact angles and the surface free energy of solids, in: R. J. Good and R. R. Stromberg (Eds.), Surface and Colloid Science, Plenum Press, New York, NY, 1979, p 1.

[37] M. Nyström, M. Laatikainen, K. Turku and P. Jarvinen, Resistance to fouling accomplished by modification of ultrafiltration membranes, Prog. Colloid Polymer Science 82 (1990) 321.

[38] G. Capannelli, A. Bottino, V. Gekas and G. Tragardh, Protein fouling behavior of ultrafiltration membranes prepared with varying degrees of hydrophilicity, (1990) 221.

[39] W. Zhang and B. Hallström, Membrane characterization using the contact angle technique, I. Methodology of the captive bubble technique, Desalination 79 (1990) 1.

[40] V. Gekas, K.M. Persson, M. Wahlgren and B. Sivik, Contact angles of ultrafiltration membranes and their possible correlation to membrane performance, Journal of Membrane Science 72 (1992) 293.

[41] A. Nabe, E. Staude and G. Belfort, Surface modification of polysulfone ultrafiltration membranes and fouling by BSA solutions, Journal of Membrane Science 133 (1997) 57.

[42] J. Cho, G. Amy and J. Pellegrino, Membrane filtration of natural organic matter: initial comparison of rejection and flux decline characteristics with ultrafiltration and nanofiltration membranes, Water Resources 33 (1999) 2517.

[43] C. Combe, E. Molis, P. Lucas, R. Riley and M.M. Clark, The effect of CA membrane properties on adsorptive fouling by humic acid, Journal of Membrane Science 154 (1999) 73.

[44] G. Capannelli, A. Bottino, V. Gekas and G. Tragardh, Protein fouling behavior of ultrafiltration membranes prepared with varying degrees of hydrophilicity, Process Biochemistry International,

[45] J.-M. Laîné, J.P. Hagstrom, M.M. Clark and J. Mallevialle, Effects of ultrafiltration membrane composition, Journal of American Water Works Association 81 (1989) 61.

[46] A. Kulkarni, D. Mukherjee and W.N. Gill, Flux enhancement by hydrophilization of thin film composite reverse osmosis membranes, Journal of Membrane Science 114 (1996) 39.

[47] K. Majewska-Nowak, M. Kabsch-Korbutowicz and T. Winnicki, Salt effect on the dye separation by hydrophilic membranes, Desalination 108 (1996) 221.

[48] D. Mukherjee, A. Kulkarni and W.N. Gill, Chemical treatment for improved performance of reverse osmosis membranes, Desalination 104 (1996) 239.

[49] M. Kabsch-Korbutowicz, K. Majewska-Nowak and T. Winnicki, Analysis of membrane fouling in the treatment of water solutions containing humic acids and mineral salts, Desalination 126 (1999) 179.

[50] P.C. Hiemenz, Principles of Colloid and Surface Chemistry, Marcel Dekker, Inc., New York, NY, 1986.

[51] J. Lindau and A.-S. Jönsson, Adsorptive fouling of modified and unmodified commercial polymeric ultrafiltration membranes, Journal of Membrane Science 160 (1999) 65.

[52] S. Belfer, Y. Purinson, R. Fainshtein, Y. Radchenko and O. Kedem, Surface modification of commercial composite polyamide reverse osmosis membranes, Journal of Membrane Science 139 (1998) 175.

[53] X. Zhu and M. Elimelech, Colloidal fouling of reverse osmosis membranes: measurements and fouling mechanisms, Environmental Science and Technology 31 (1997) 3654.

[54] S. Hong, R.S. Faibish and M. Elimelech, Kinetics of permeate flux decline in crossflow membrane filtration of colloidal suspensions, Journal of Colloid and Interface Science 196 (1997) 267.

[55] S. Bhattacharjee, J.Y. Chen and M. Elimelech, DLVO interaction energy between spheroidal particles and a flat surface, Colloids and Surfaces A: Physicochemical and Engineering Aspects 165 (2000) 143.

[56] W.C. Hamilton, A technique for the characterization of hydrophilic surfaces, Journal of Colloid and Interface Science 40 (1971) 219.

[57] M. Oldani and G. Schock, Characterization of ultrafiltration membranes by infrared spectroscopy, ESCA, and contact angle measurements, Journal of Membrane Science 43 (1989) 243.

[58] K. Grundke, T. Bogumil, C. Werner, A. Janke, K. Pöschel and H.-J. Jacobasch, Liquid-fluid contact angle measurements on hydrophilic cellulosic materials, Colloids and Surfaces A: Physiochemical and Engineering Aspects 116 (1996) 79.

[59] M.J. Rosa and M.N. Pinho, Membrane surface characterization by contact angle measurements using the immersed method, Journal of Membrane Science 131 (1997) 167.

[60] E.L. Decker, B.P. Frank, Y. Suo and S. Garoff, Physics of contact angle measurement, Colloids and Surfaces A: Physiochemical and Engineering Aspects 156 (1999) 177.

[61] G. Wolanksky and A. Marmur, The actual contact angle on a heterogeneous rough surface in three dimensions, Langmuir 14 (1998) 5292.

[62] C.W. Extrand, A thermodynamic model for contact angle hysteresis, Journal of Colloid and Interface Science 207 (1998) 19.

[63] D.Y. Kwok, R. Lin, M. Mui and A.W. Neumann, Low-rate dynamic and static contact angles and the determination of solid surface tensions, Colloids and Surfaces A: Physiochemical and Engineering Aspects 116 (1996) 63.

[64] D.Y. Kwok and A.W. Neumann, Contact angle measurement and contact angle interpretation, Advances in Colloid and Interface Science 81 (1999) 167.

[65] F.M. Fowkes, Ind. Eng. Chem. 56 (1964) 40.

[66] C.J. van Oss, R.J. Good and M.K. Chaudhury, Solubility of proteins, Journal of Protein Chemistry 5 (1986) 385.

[67] C.J. van Oss and R.J. Good, Orientation of the water molecules of hydration of human serum albumin, Journal of Protein Chemistry 7 (1988) 179.

[68] C.J. van Oss, M.K. Chaudhury and R.J. Good, Interfacial Lifshitz-van der Waals and polar interactions in macroscopic systems, Chemical Reviews 88 (1988) 927.

[69] A. Marmur, Equilibrium contact angles: theory and measurement, Colloids and Surfaces A: Physiochemical and Engineering Aspects 116 (1996) 55.

[70] J. Drelich and J.D. Miller, The effect of solid surface heterogeneity and roughness on the contact angle/drop (bubble) size relationship, Journal of Colloid and Interface Science 164 (1994) 252.

[71] C.W. Extrand and Y. Kumagai, Contact angles and hysteresis on soft surfaces, Journal of Colloid and Interface Science 184 (1996) 191.

[72] R.J. Good and M.N. Koo, The effect of drop size on contact angle, Journal of Colloid and Interface Science 71 (1979) 283.

[73] J.T.F. Keurentjes, J.G. Harbrecht, D. Brinkman, J.H. Hanemaaijer, M.A. Cohen Stuart and K. van't Riet, Hydrophobicity measurements of microfiltration and ultrafiltration membranes, Journal of Membrane Science 47 (1989) 333.

[74] J. Drelich, J.D. Miller and R.J. Good, The effect of drop (bubble) size on advancing and receding contact angles for heterogeneous and rough solid surfaces as observed with sessile-drop and captive-bubble techniques, Journal of Colloid and Interface Science 179 (1996) 37.

[75] C.J. van Oss, A. Docoslis, W. Wu and R.F. Giese, Influence of macroscopic and microscopic interactions on kinetic rate constants: I. Role of the extended DLVO theory in determining the kinetic adsorption constant of proteins in aqueous media, using von Smoluchowski's approach, Colloids and Surfaces B: Biointerfaces 14 (1999) 99.

[76] C.J. van Oss, Hydrophobic, hydrophilic and other interactions in epitope-paratope binding, Molecular Immunology 32 (1995) 199.

[77] S. Bhattacharya and S.T. Hwang, Concentration polarization, separation factor, and Peclet number in membrane processes, Journal of Membrane Science 132 (1997) 73.

[78] R.I. Hogg, T.W. Healy and D.W. Fuerstenau, Mutual coagulation of colloidal dispersions, Transactions of the Faraday Society 62 (1966) 1638.

[79] A.E. Childress and M. Elimelech, Effect of solution chemistry on the surface charge of polymeric reverse osmosis and nanofiltration membranes, Journal of Membrane Science 119 (1996) 253.

[80] A. Szymczyk, P. Fievet, J.C. Reggiani and J. Pagetti, Characterisation of surface properties of ceramic membranes by streaming and membrane potentials, Journal of Membrane Science 146 (1998) 277.

[81] A.E. Childress and S.S. Deshmukh, Effect of humic substances and anionic surfactants on the surface charge and performance of reverse osmosis membranes, Desalination 118 (1998) 167.

[82] J. Cho, G. Amy, J. Pellegrino and Y. Yoon, Characterization of clean and natural organic matter (NOM) fouled NF and UF membranes, and foulants characterization, Desalination 118 (1998) 101.

[83] M. Elimelech, W.H. Chen and J.J. Waypa, Measuring the zeta (electrokinetic) potential of reverse osmosis membranes by a streaming potential analyzer, Desalination 95 (1994) 269.

[84] A. Pihlajamäki, Electrochemical characterization of filter media properties and their exploitation in enhanced filtration, Lappeenranta University of Technology, Doctoral Dissertation, Lappeenranta, Finland (1998).

[85] H.J. Busscher, A.W.J. Van Pelt, P. DeBeer, H.P. De Jong and J. Arends, The effect of surface roughening of polymers on measured contact angles of liquids, Colloids and Surfaces 9 (1984) 319.

[86] A.E. Childress and M. Elimelech, Relating nanofiltration membrane performance to membrane charge (electrokinetic) characteristics, Environmental Science and Technology 34 (2000) 3710.

[87] R.J. Hunter, Foundations of Colloid Science Vol. I, Oxford University Press, New York, NY, 1986.